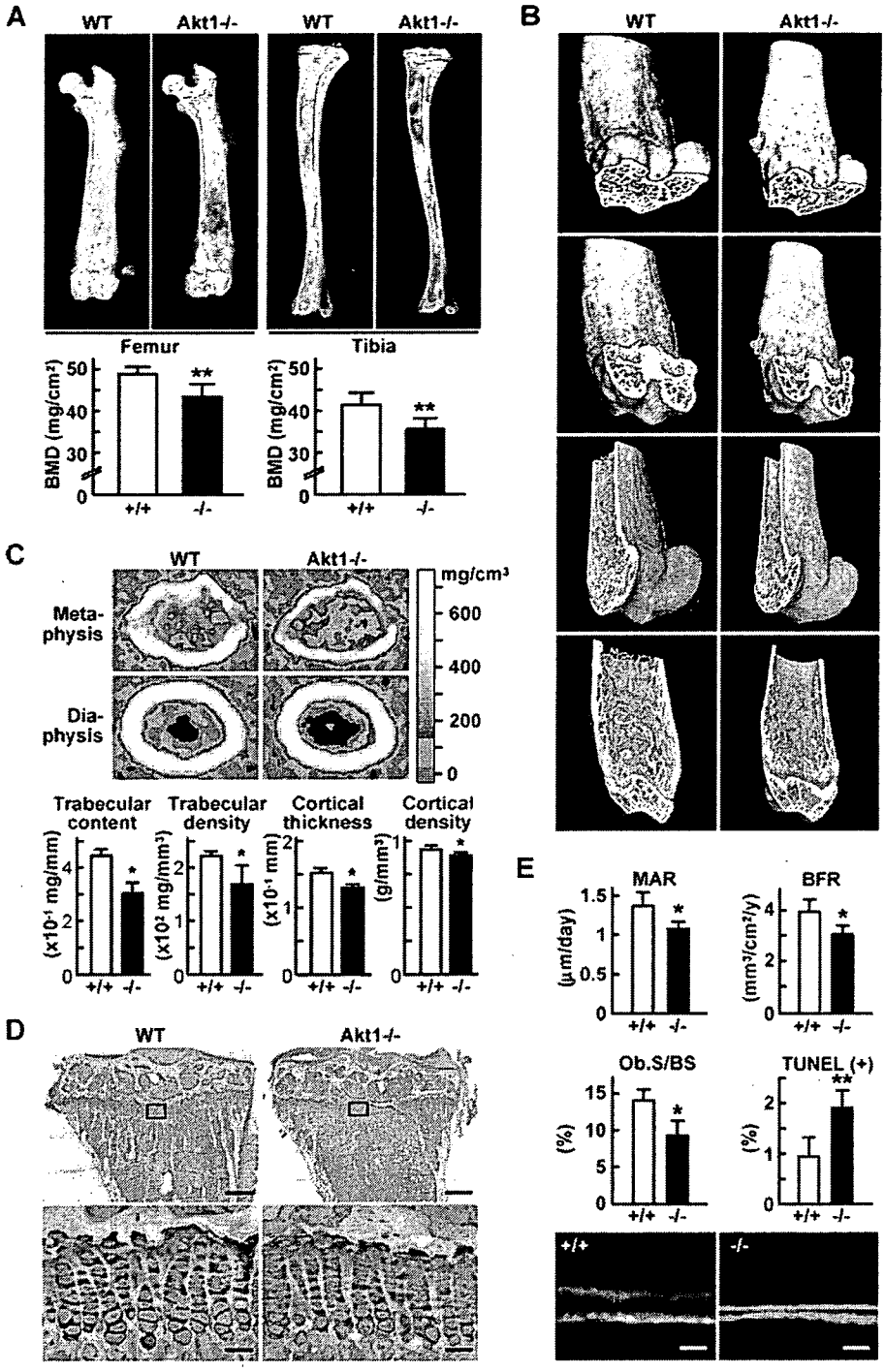

Figure 1. Bone mass and formation are decreased in Akt1-/- mice. (A) Plain X-ray images of femur and tibia in WT and Akt1-/- male littermates at 8 weeks of age. The BMD of the entire femurs and tibias measured by DXA is shown in the graphs below. Data are expressed as means (bars)±SEM (error bars) for 5 WT and 3 Akt1-/- littermates. **P<0.01 vs. WT. (B) Three-dimensional CT images of distal femurs. (C) pQCT images of the distal metaphysis and the mid-diaphysis of the femurs. The color gradient indicating BMD is shown in the right bar. The trabecular content and density at the metaphysis, and the cortical thickness and density at the diaphysis are shown in the graphs below. Data are expressed as means (bars)±SEM (error bars) for 4 mice/group. *P<0.05 vs. WT. (D) Toluidine blue staining of the proximal tibias. Inset boxes indicate the regions of the bottom figures. The growth plate heights were 94.7±2.9 and 95.8±3.8 μm for WT and Akt1-/-, respectively (mean±SEM of 4 mice/group). Bars, 200 μm (top)&30 μm (bottom). (E) Bone formation parameters in histomorphometric analysis at the proximal tibias. MAR, mineral apposition rate; BFR/BS, bone formation rate per bone surface; Ob.S/BS, osteoblast surface per bone surface; TUNEL(+), percentage of TUNEL-positive apoptotic osteoblasts. Data are expressed as means (bars)±SEM (error bars) for 3–4 mice/group. *P<0.05, **P<0.01 vs. WT. The bottom figures show the representative calcein double labelings; bars, 20 μm.

doi:10.1371/journal.pone.0001058.g001

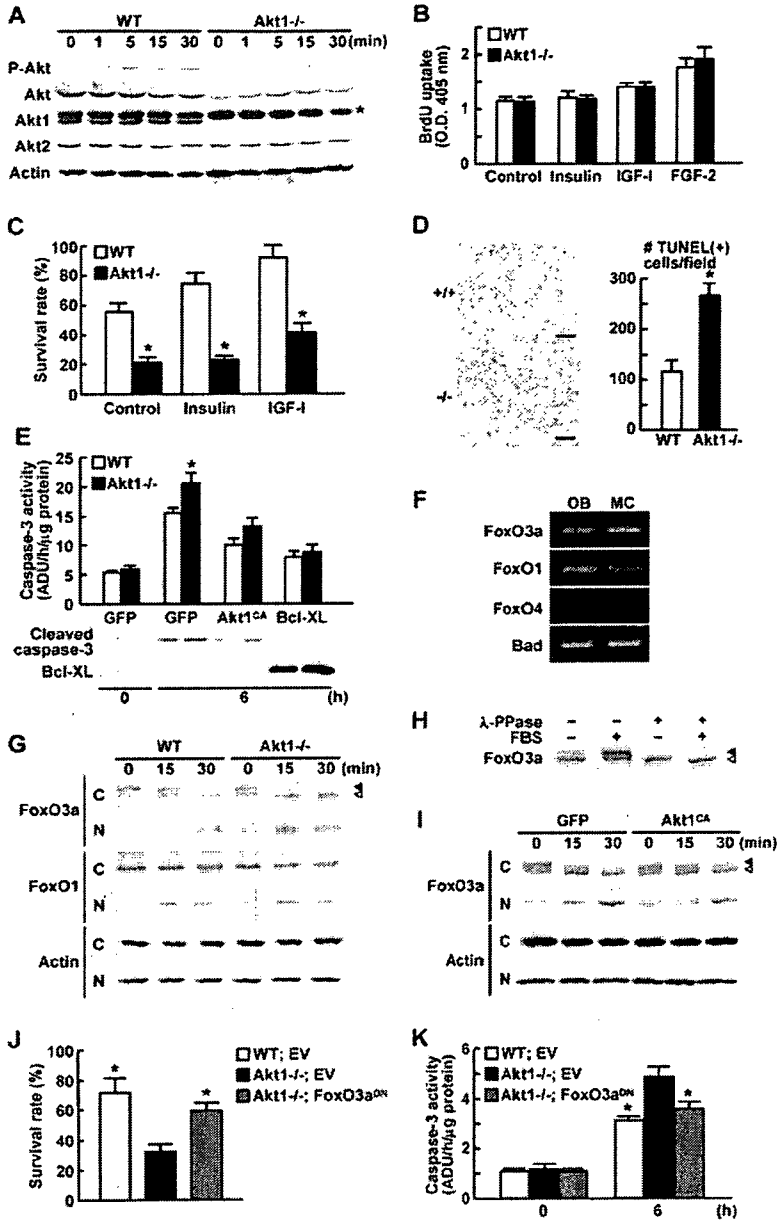

Figure 2. Akt1-/- osteoblasts are susceptibile to apoptosis via FoxO3a. (A) Time course of phosphorylated total Akt (P-Akt), total Akt (Akt), Akt1, Akt2, and β-actin levels after IGF-I stimulation determined by Western blotting in cultured calvarial osteoblasts from WT and Akt1-/- mice. An asterisk indicates a nonspecific band detected by an antibody to Akt1. (B) Cell proliferation determined by BrdU uptake into calvarial osteoblasts of two genotypes cultured with and without insulin, IGF-I, or FGF-2. Data are expressed as means (bars)±SEM (error bars) for 6 wells/group. (C) Survival rate of WT and Akt1-/- osteoblasts 48 h after serum deprivation in cultures with and without insulin or IGF-I. Data are expressed as means (bars)±SEM (error bars) for 6 wells/group. *P<0.01 vs. WT. (D) The number of TUNEL-positive osteoblasts per field (6×10^5 μm^2) 24 h after serum deprivation in cultured calvarial osteoblasts. Data are expressed as means (bars)±SEM (error bars) of 3 wells/group. *P<0.01 vs. WT. Bars, 100 μm. (E) Caspase-3 activity (top graph) and Western blotting for cleaved caspase-3 and Bcl-x_L (bottom) in WT and Akt1-/- osteoblasts adenovirally transfected with GFP, Akt1^{CA}, and Bcl-x_L before and 6 h after serum deprivation. Data are expressed as means (bars)±SEM (error bars) for 3 wells/group. *P<0.05 vs. WT. ADU: arbitrary densitometry unit. (F) FoxO3a, FoxO1, FoxO4 and Bad expressions determined by RT-PCR in primary mouse calvarial osteoblasts (OB) and MC3T3-E1 cells (MC). (G) Time course of FoxO3a, FoxO1, and β-actin levels by Western blotting after serum deprivation in the cytoplasmic (C) and nuclear (N) fractions of cultured WT and Akt1-/- osteoblasts. Closed and open arrowheads indicate phosphorylated and unphosphorylated FoxO3a, respectively. (H) Western blotting for FoxO3a in the cytoplasmic fraction of WT osteoblasts cultured with and without 10% FBS for 30 min. The lysates were treated with and without lambda protein phosphatase (λ-PPase). (I) Time course of FoxO3a and β-actin levels by Western blotting after serum deprivation in the cytoplasmic (C) and nuclear (N) fractions of cultured osteoblasts adenovirally transfected with GPF or Akt1^{CA}. (J) Survival rate of WT and Akt1-/- osteoblasts retrovirally transfected with empty vector (EV) or FoxO3a^{DN} 48 h after serum deprivation. Data are expressed as means (bars)±SEM (error bars) for 6 wells/group. *P<0.05 vs. Akt1-/- with EV. (K) Caspase-3 activity of WT and Akt1-/- osteoblasts retrovirally transfected with EV or FoxO3a^{DN} before and 6 h after serum deprivation. Data are expressed as means (bars)±SEM (error bars) for 3 wells/group. *P<0.05 vs. Akt1-/- with EV. ADU: arbitrary densitometry unit.
doi:10.1371/journal.pone.0001058.g002

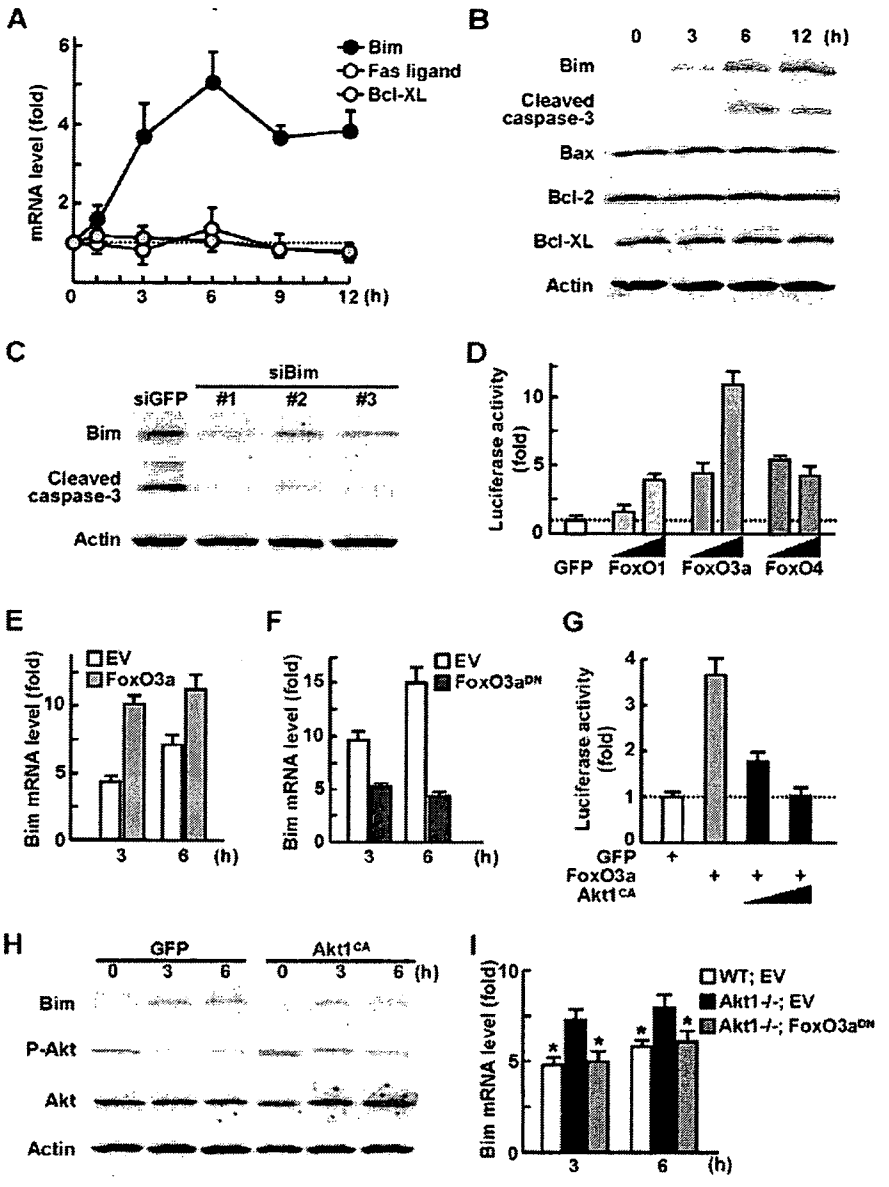

Figure 3. Akt1 suppresses osteoblast apoptosis via inhibition of FoxO3a and Bim. (A) Time course of mRNA levels determined by real-time RT-PCR of Bim, Fas ligand, and Bcl-x_L after serum deprivation in cultured calvarial osteoblasts. Data are normalized to those of β-actin and are expressed as means (symbols)±SEM (error bars) of the relative amount compared to time 0. (B) Time course of Bim, cleaved caspase-3, Bax, Bcl-2, Bcl-x_L, and β-actin levels determined by Western blotting after serum deprivation in cultured calvarial osteoblasts. (C) Western blotting for Bim, cleaved caspase-3, and β-actin levels 6 h after serum deprivation in MC3T3-E1 cells retrovirally transfected with three kinds of Bim siRNA or the control GFP siRNA. (D) Bim promoter activity determined by luciferase reporter assay in cultured MC3T3-E1 cells transfected with luciferase reporter constructs containing a 2-Kb Bim 5′-end flanking region. Plasmid vectors of the control GFP, FoxO1, FoxO3a, and FoxO4 were co-transfected in increasing amounts. Data are expressed as means (bars)±SEM (error bars) of the fold change compared to GFP. (E, F) Bim mRNA level determined by real-time RT-PCR 3 h and 6 h after serum deprivation in MC3T3-E1 cells retrovirally transfected with FoxO3a (E), FoxO3a^{DN} (F), or the respective EV. Data are normalized to those of β-actin and are expressed as means (bars)±SEM (error bars) of the relative amount compared to time 0. (G) Bim promoter activity analysis in MC3T3-E1 cells transfected with the control GFP, FoxO3a, and Akt1^{CA} plasmid vectors in increasing amounts. Data are expressed as means (bars)±SEM (error bars) of the fold change compared to GFP. (H) Time course of Bim, phosphorylated total Akt (P-Akt), total Akt (Akt), and β-actin levels determined by Western blotting after serum deprivation in cultured calvarial osteoblasts adenovirally transfected with GPF or Akt1^{CA}. (I) Bim mRNA level determined by real-time RT-PCR 3 h and 6 h after serum deprivation in cultured WT and Akt1-/- osteoblasts retrovirally transfected with EV or FoxO3a^{DN}. Data are normalized to those of β-actin and are expressed as means (bars)±SEM (error bars) of the relative amount compared to time 0. *$P<0.05$ vs. Akt1-/- with EV.

doi:10.1371/journal.pone.0001058.g003

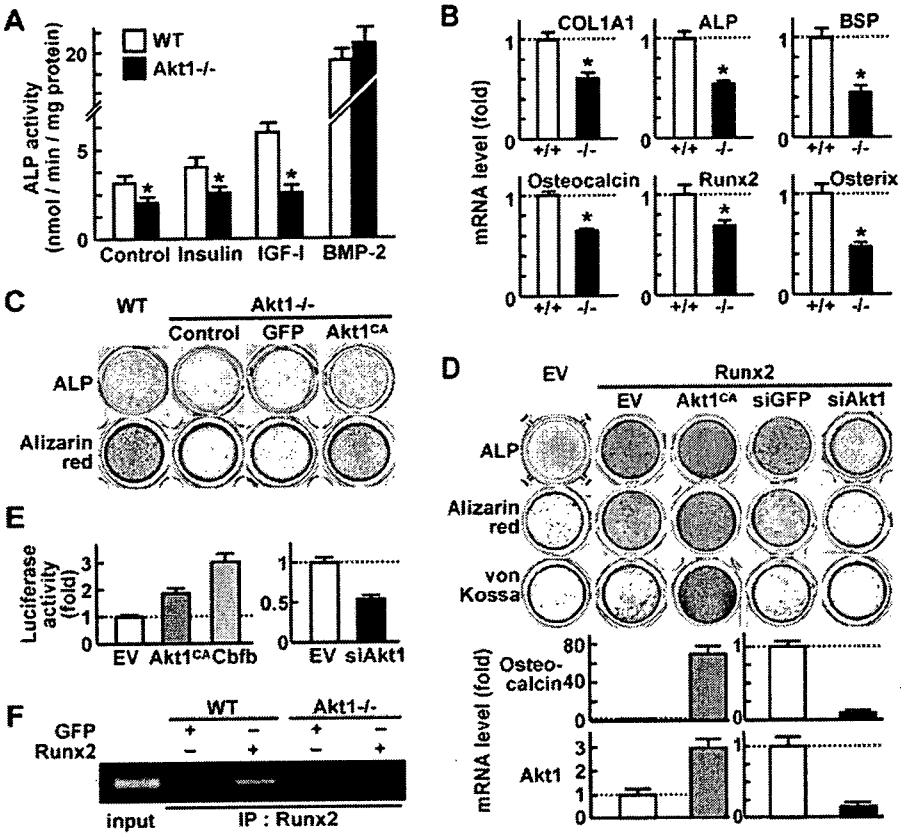

Figure 4. Akt1 enhances Runx2-dependent osteoblast differentiation and function. (A) ALP activity of WT and Akt1-/- osteoblasts cultured with and without insulin, IGF-I or BMP-2. Data are expressed as means (bars)±SEM (error bars) for 4 wells/group. *P<0.05 vs. WT. (B) mRNA levels of type I collagen (COL1A1), ALP, bone sialoprotein (BSP), osteocalcin, Runx2, and osterix in WT and Akt1-/- osteoblasts determined by real-time RT-PCR. Data are normalized to those of β-actin and are expressed as means (bars)±SEM (error bars) of the relative amount compared to WT culture. *P<0.01 vs. WT. (C) ALP and Alizarin red stainings of WT and Akt1-/- osteoblasts with and without adenoviral transfection of GFP or Akt1^{CA}. (D) ALP, Alizarin red, and von Kossa stainings of MC3T3-E1 cells retrovirally transfected with Runx2 or the empty vector (EV). Runx2 transfectants were retrovirally co-transfected with Akt1^{CA} or the control EV, and Akt1 siRNA (siAkt1) or the control (siGFP). The graphs indicate mRNA levels of osteocalcin and Akt1 determined by real-time RT-PCR. Data are normalized to those of β-actin and are expressed as means (bars)±SEM (error bars) of the relative amount compared to the control culture. (E) Osteocalcin promoter activity in retroviral Runx2 transfectants of MC3T3-E1 cells that were transfected with luciferase reporter constructs containing a 1,050 bp osteocalcin 5'-end flanking region. Plasmid vectors of Akt1^{CA}, the negative control EV, and the positive control Cbfb that is a representative co-activator of Runx2, as well as those of siAkt1 and the control EV were co-transfected. Data are expressed as means (bars)±SEM (error bars) of the fold change compared to EV. (F) ChIP assay using cell lysates of WT and Akt1-/- osteoblasts adenovirally transfected with GFP or Runx2. Purified DNA from with (IP) and without (input) immunoprecipitation by an antibody to Runx2 was amplified by PCR using a primer set in the mouse osteocalcin promoter region (−471/−67).
doi:10.1371/journal.pone.0001058.g004

introduction failed to commit immature mesenchymal cell lines C2C12 and C3H10T1/2 to osteoblastic lineage, although Runx2, a master transcription factor for osteoblastic differentiation, potently induced it (Supp. Fig S5).

These results suggest that Akt1 does not induce Runx2 expression but acts instead on differentiated osteoblasts that have the potency to express Runx2. Hence, as a possible mechanism underlying the osteogenic action of Akt1, we looked at its modulation of Runx2 function. Akt1 overexpression by Akt1^{CA} introduction into Runx2 stable transfectants of MC3T3-E1 cells enhanced the Runx2 activity on osteoblast differentiation and function, and vice versa, while Akt1 silencing by the siRNA introduction attenuated them (Fig 4D). Promoter activity of osteocalcin, a representative transcriptional target of Runx2, in Runx2-overexpressing MC3T3-E1 cells was also enhanced by Akt1^{CA} and suppressed by Akt1 siRNA (Fig 4E). Chromatin immunoprecipitation (ChIP) showed that the complex of Runx2 and osteocalcin promoter seen in WT osteoblasts disappeared in Akt1-/- osteoblasts (Fig 4F). Collectively, Akt1 is likely to enhance the Runx2-dependent osteoblast differentiation and function through enhancement of the DNA binding and the transcriptional activity.

Akt1 deficiency impairs bone resorption via dysfunctions of osteoclasts and osteoblasts

Finally, we investigated the role of Akt1 in bone resorption. The number of osteoclasts determined by tartrate-resistant acid phosphatase (TRAP) staining was reduced in the Akt1-/- bone in vivo (Fig 5A), which was confirmed by decreased bone

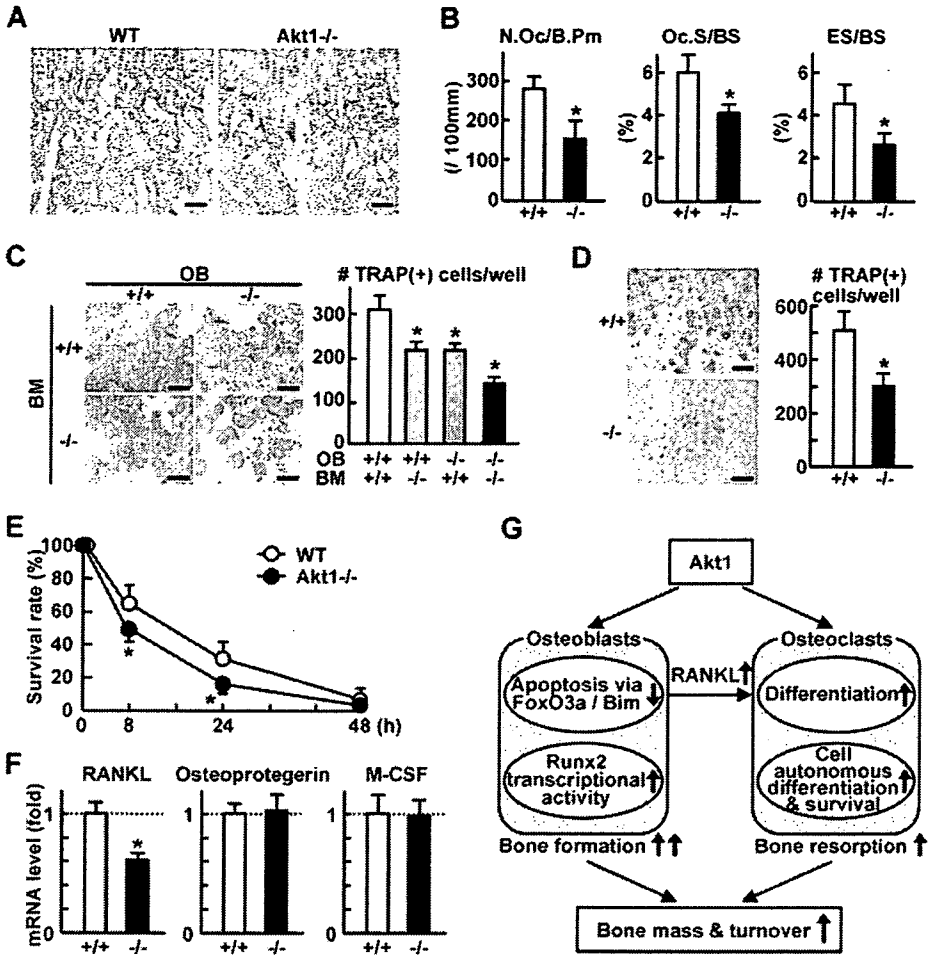

Figure 5. Akt1 deficiency impairs bone resorption via dysfunctions of osteoclasts and osteoblasts. (A) TRAP staining of proximal tibias of 8 week-old WT and Akt1-/- mice. Bars, 100 μm. (B) Bone resorption parameters in histomorphometric analysis at the secondary spongiosa of the proximal tibias. N.Oc/B. Pm, number of osteoclasts per 100 mm of bone perimeter; Oc.S/BS, osteoclast surface per bone surface; ES/BS, eroded surface per bone surface. Data are expressed as means (bars)±SEM (error bars) for 3–4 mice/group. *P<0.05 vs. WT (+/+). (C) The number of TRAP-positive multinucleated osteoclasts formed in the coculture of osteoblasts (OB) and bone marrow cells (BM) from WT or Akt1-/- littermates. Data are expressed as means (bars)±SEM (error bars) for 4 wells/group. *P<0.05 vs. WT. Bars, 500 μm. (D) The number of TRAP-positive multinucleated osteoclasts formed from BMM cultured in the presence of RANKL and M-CSF. Data are expressed as means (bars)±SEM (error bars) for 4 wells/group. *P<0.01 vs. WT. Bars, 200 μm. (E) Time course of survival rate of mature osteoclasts after deprivation of RANKL and M-CSF. Mature osteoclasts were formed from BMM in the presence of RANKL and M-CSF. Data are expressed as means (symbols)±SEM (error bars) for 4 wells/group. *P<0.05 vs. WT. (F) mRNA levels of RANKL, osteoprotegerin, and M-CSF in cultured osteoblasts by real-time RT-PCR. Data are normalized to those of β-actin and are expressed as means (bars)±SEM (error bars) of the relative amount compared to the WT culture. *P<0.01 vs. WT. (G) Schematic diagram of the mechanisms underlying the Akt1 function to maintain bone mass and turnover. Akt1 suppresses the susceptibility to mitochondria-dependent apoptosis of osteoblasts by inhibiting the FoxO3a nuclear entry and the Bim transactivation, and stimulates the differentiation and function by enhancing the Runx2 transcriptional activity, resulting in increased bone formation. Akt1 also induces RANKL expression in osteoblasts to support osteoclast differentiation, and shows cell-autonomous defects in osteoclasts to stimulate the differentiation and survival, resulting in increased bone resorption.
doi:10.1371/journal.pone.0001058.g005

resorption parameters in the histomorphometric analysis (Fig 5B). Osteoclastogenesis in the ex vivo co-culture was reduced when either osteoblasts or bone marrow cells were derived from Akt1-/- mice, and was additively reduced when both were from Akt1-/- (Fig 5C). This indicates that Akt1 is necessary for osteoclast precursors in a cell autonomous manner and for osteoblasts to support osteoclast differentiation. Osteoclastogenesis in the culture of osteoclast-progenitor BMM derived from Akt1-/- was suppressed even in the presence of soluble receptor activator of nuclear factor κB ligand (RANKL) and M-CSF (Fig 5D). Furthermore, the survival of mature osteoclasts formed from Akt1-/- BMM was also impaired (Fig 5E), confirming that the intrinsic Akt1 in osteoclastic cells is necessary to maintain bone resorptive function. Contrarily, decreased expression of RANKL, but not osteoprotegerin or M-CSF, in Akt1-/- osteoblasts (Fig 5F) explains the contribution of Akt1 in osteoblasts to osteoclastic bone resorption.

Taken together, Akt1 deficiency may cause impairment of bone resorption via the cell autonomous dysfunction in osteoclasts and the cell non-autonomous inhibition of osteoclastogenesis due to reduced RANKL expression in osteoblasts.

DISCUSSION

Physiological roles of Akt1 in bone

The present study initially analyzed the bones of mice lacking Akt1 and found that the deficiency caused osteopenia with a low turnover state. Further in vivo and ex vivo analyses of osteoblasts and osteoclasts revealed that the Akt1 deficiency caused impairments of both bone formation and bone resorption via respective cell autonomous mechanisms (Fig 5G). The imbalance between formation and resorption, the underlying mechanism of which remains to be clarified, may cause osteopenia with a low bone turnover.

Akt1 in osteoblasts

Akt1 deficiency in osteoblasts caused three cell autonomous abnormalities: increased susceptibility to apoptosis, suppressed differentiation and function, and decreased RANKL expression to support osteoclastogenesis. Most notably among them, the enhanced apoptosis in Akt1-/- osteoblasts was shown to be mitochondria-dependent via the FoxO3a nuclear entry and the Bim transactivation. A recent report on mice with osteoblast-specific deletion of phosphatase and tensin homolog (Pten) demonstrated reduced osteoblast apoptosis and increased bone mass by constitutive activation of Akt signaling, corresponding to the present finding, although the downstream molecular mechanism remained unclarified [18]. The candidates of substrates of Akt1 included caspase-9, Bad, and FoxOs whose involvement in mitochondria-dependent apoptosis had been established in other cells [9]. Although caspase-9 functions as one of the most important effectors in the apoptosis, the lack of a minimal substrate consensus sequence for Akt [9] led us to exclude this from the candidates. A proapoptotic molecule Bad was expressed in osteoblasts, but the phosphorylation could not be detected. FoxO proteins identified in mammals, FoxO1, FoxO3a and FoxO4, constitute a newly characterized subfamily of the Forkhead/winged helix group of transcription factors and play a predominant role in mediating various functions of the PI3K/Akt pathway [16,17]. Although disruption of the genes in mice has revealed the necessities of FoxO1 in embryonic vessel formation and FoxO3a in ovarian follicular development [19], their roles in bone metabolism remained unknown. This study showed expressions of FoxO1 and FoxO3a, but not FoxO4, in osteoblasts, and functional involvement of FoxO3a in their survival as a phosphorylation target of Akt1. Contrarily, the nuclear entry of FoxO1 after serum deprivation was independent of Akt1 (Fig 2G), implicating that different isoforms of Akt may have specific preference to FoxO proteins as the substrates. In fact, similarly to Akt2, FoxO1 is expressed predominantly in insulin target tissues and regulates their insulin resistance [16].

Bim, Bcl-2-interacting mediator of cell death, was shown to be a transcriptional target of FoxO3a that lies downstream of the Akt1 anti-apoptotic signaling in osteoblasts. Proapoptotic activity of Bim is regulated both transcriptionally and post-transcriptionally [20], and the transcriptional induction is known to be mediated by FoxOs under the apoptotic stimulation in other cells [17,21–23]. Studies on knockout mice have revealed that Bim is essential for apoptosis of lymphocytes, myeloid cells, neurons, and osteoclasts [24,25]. Regarding osteoblast apoptosis, the involvement of Bcl-2 family proteins such as Bax and Bcl-2 has been reported [7,26]. Because the changes in protein levels of these molecules are crucial for osteoblast apoptosis, these changes seem to be independent of the Bim regulation.

Suppressed differentiation and function in Akt1-/- osteoblasts was shown to be mediated at least partly by modulating the Runx2 activity. The present results using Akt1-null materials confirmed a previous report by Fujita et al. that gain- and loss-of-functions of PI3K/Akt signaling regulate the DNA binding and transactivity of Runx2 in cultures of osteoblastic cells [27]. Since Runx2 does not have a consensus sequence for Akt phosphorylation, Akt is not likely to phosphorylate Runx2 directly, but may regulate the activity or stability of co-activators or co-repressors of Runx2. However, the fact that Akt1-/- mice did not exhibit cleidocranial dysplasia (Supp. Fig S2B), the characteristic phenotype of Runx2+/− mice, indicates that Akt1 is not a crucial regulator of the Runx2-dependent bone formation in vivo.

Akt1 in osteoclasts

Besides the defects in osteoblasts, the deficiency of Akt1 in osteoclasts caused impairment of bone resorption via the cell autonomous dysfunction. To date, the role of Akt signaling in osteoclasts has been controversial. RANKL and M-CSF have been reported to promote the osteoclast survival in part by activating the Akt pathway [28,29]. Contrarily, Akt is shown to be dispensable for the survival by knockdown experiment using Akt1/Akt2 siRNA, but is necessary for the proliferation and differentiation [30]. Our results using ex vivo cultures of isolated Akt1-/- osteoclasts have provided genetic evidence that Akt1 signaling promotes the differentiation and survival. The regulation of differentiation might be dependent on the DNA binding of NFκB, since previous knockdown studies of Akt1 and/or Akt2 showed inhibition of RANKL-induced NFκB p50 DNA-binding activity via IκB kinase α [30].

By analogy with osteoblasts, the enhanced osteoclast survival by Akt1 might be mediated by the FoxO3a/Bim axis, since Bim is reported to be critical for osteoclast apoptosis [25]. However, this is dependent on post-transcriptional regulation by ubiquitylation and proteasomal degradation of Bim mediated by ERK pathway, but not on transcriptional regulation as seen in the case of osteoblast apoptosis. In addition, Bim in osteoclasts stimulates not only the apoptosis, but also the bone resorptive activity. If Bim is enhanced in Akt1-/- osteoclasts just as in the osteoblasts, the bone resorption parameters like eroded surface are assumed to increase. Hence, the mechanism by which Akt1 suppresses apoptosis in osteoclasts is likely to be different from that in osteoblasts. The cell autonomous mechanism of Akt1 in osteoclasts is the next task we intend to pursue.

Akt1 as a mediator of bone anabolic signaling

Akt1 may mediate the osteoblastic bone formation by IGF-I and insulin, since their effects on osteoblast survival and differentiation were impaired in Akt1-/- osteoblasts (Fig 2C, 4A). Contrarily, although BMP-2 induced phosphorylation of the entire Akt (Supp. Fig S1A), the stimulated osteoblast differentiation was not affected by the Akt1 deficiency (Fig 4A), suggesting the mediation of other Akt isoforms or other pathways in the BMP-2 signaling. IGF-I is known to function as a potent bone anabolic factor via autocrine/paracrine and endocrine mechanisms [4], since skeletal and serum IGF-I levels were positively correlated with bone density between two inbred strains of mice [31]. Serum IGF-I levels of Akt1-/- mice were comparable to that of WT in the age from 8 to 16 weeks (data not shown), suggesting the absence of reduced IGF-I secretion or systemic compensation for impaired IGF-I signaling. Hence, the decreased bone formation in vivo in Akt1-/- mice may be at least in part due to the deficit of anabolic IGF-I signaling. Considering that Akt1; Akt2 double-knockout mice and IGF-I receptor knockout mice exhibit similar phenotypes [14,32], Akt may be the main mediator of the IGF-I signaling. Bone anabolic

action of other hormones like parathyroid hormone, growth hormone, and thyroid hormone are reported to be mediated by IGF-I signaling [33–36], and it is possible that the IGF-I/Akt1 pathway might be a common pathway for actions of these major hormones in bone.

As presented herein, Akt1, a multifaceted kinase which mediates various kinds of upstream signals to a diverse spectrum of substrates, plays multiple roles in bone cells as well as other cell types reported. Although it seems difficult to target this molecule directly in order to yield novel therapeutics for bone disorders because of its ubiquitous expression and diverse functions, further understanding of the molecular network related to Akt1 will greatly help us to unravel the complex mechanism modulating bone remodeling.

MATERIALS AND METHODS

Mice

The generation of Akt1-/- mice was described previously [11]. All mice were maintained in the C57BL/6 background with a standard diet. In each experiment, homozygous WT and Akt1-/- mice that were littermates generated from the intercross between heterozygous mice were compared. All experiments were performed on 8-week-old male mice unless otherwise described, according to the protocol approved by the Animal Care and Use Committee of the University of Tokyo.

Radiological analyses

Plain radiographs were taken using a soft X-ray apparatus (CMB-2, SOFTEX), and the BMD was measured by dual energy X-ray absorptiometry (DXA) using a bone mineral analyzer (PIXImus Densitometer, GE Medical Systems). CT scanning of the femurs was performed using a composite X-ray analyzer (NX-CP-C80H-IL, Nittetsu ELEX Co.), and reconstructed into a 3D feature by the volume-rending method (VIP-Station, Teijin System Technology). pQCT scan was performed at the metaphysis 1.4 mm above the distal growth plate and at the mid-shaft of femurs.

Histological analyses

For toluidine blue staining, samples were fixed with 70% ethanol, embedded in methyl methacrylate, and sectioned in 6-μm slices. Histomorphometric analyses were performed as described [37] in the growth plate and secondary spongiosa (1.2 mm in length from 0.5 mm below the growth plate) of the proximal tibias, according to the ASBMR nomenclature report [38]. For double labeling of the mineralization front, mice were injected subcutaneously with 16 mg/kg body weight of calcein at 5 d and 1 d before sacrifice. TRAP-positive cells were stained at pH 5.0 in the presence of L (+)-tartaric acid using naphthol AS-MX phosphate (Sigma-Aldrich) in *N,N*-dimethyl formamide as the substrate. Apoptotic osteoblasts were detected by TUNEL method using an ApopTag Peroxidase In Situ Apoptosis Detection Kit (Chemicon) on paraffin-embedded sections of neonate mice. The percentage of apoptotic cells was calculated by dividing the number of TUNEL-positive cells by the number of counted cells. A total of at least 400 osteoblasts were counted in each section, and five to seven sections per group were analyzed.

Osteoblastic cell cultures and assays

For osteoblast cultures, calvariae of neonatal mice were digested by 0.1% collagenase and 0.2% dispase 5 times, and cells isolated by the last 3 digestions were combined and cultured in α-minimal essential medium (α-MEM) containing 10% FBS. Mouse osteoblastic MC3T3-E1 cells were cultured in the same way. Immature mesenchymal C2C12 cells and C3H10T1/2 cells were cultured in Dulbecco's modified Eagle's medium (DMEM) supplemented with 10% FBS. Cell proliferation was determined using a BrdU Labeling and Detection Kit III (Roche Diagnostics). After 24 h culture in the presence and absence of insulin (100 nM), IGF-I (10 nM), or FGF-2 (1 nM), the cells were labeled with BrdU for an additional 4 h, and BrdU uptake was detected following the manufacturer's instructions. To determine the osteoblast apoptosis, the culture medium was changed to a serum-free one with and without insulin or IGF-I, and total RNA or protein was collected after designated times for subsequent assays. Cell survival was determined by counting viable cell numbers using the Cell Counting Kit-8 (Dojindo Molecular Technologies). Apoptotic osteoblasts were further detected by TUNEL staining as described above. Caspase-3 activity was measured via colorimetric detection of the cleavage of caspase-specific substrates using an APOPCYTO Caspase-3 Colorimetric Assay Kit (MBL International Co.). For ALP activity measurement, primary osteoblasts were inoculated at a density of 5×10^4 cells/well in a 24-multiwell plate and cultured in α-MEM containing 10% FBS and 50 μg/ml ascorbic acid. After 14 d of culture in the presence and absence of insulin (100 nM), IGF-I (10 nM), or BMP-2 (30 ng/ml), cells were sonicated in 10 mM Tris-HCl buffer (pH 8.0) containing 1 mM $MgCl_2$ and 0.5% Triton X-100. ALP activity in the lysate was measured using an ALP Kit (Wako Pure Chemical). Protein concentrations of cell lysates were measured with a Protein Assay Kit II (BIO-RAD). For ALP staining, cells were fixed in 70% ethanol and stained for 10 min with a solution containing 0.01% naphthol AS-MX phosphate, 1% *N,N*-dimethyl formamide, and 0.06% fast blue BB (Sigma-Aldrich). For Alizarin red S and von Kossa staining, osteoblasts were inoculated at a density of 1×10^5 cells/well in a 12-multiwell plate in α-MEM containing 10% FBS and 50 μg/ml ascorbic acid and 10 mM β-glycerophosphate (Sigma-Aldrich). On day 21 after confluency, cultured cells were fixed in 10% buffered formalin and stained for 10 min with 2% Alizarin red S (pH 4.0) (Sigma-Aldrich). For von Kossa staining, cells were fixed with 100% ethanol at room temperature for 15 min, stained with 5% silver nitrate solution under ultraviolet light for 10 min, and incubated for 5 min with 5% sodium thiosulfate solution.

Assays for osteoclastic cells

To study the role of Akt1 intrinsic to osteoclastic cells, we used a coculture of osteoblasts and bone marrow cells and the M-CSF-dependent BMM culture system as described previously [39]. Bone marrow cells were collected from long bones of 8-wk-old WT or Akt1-/- littermates. TRAP-positive multinucleated osteoclasts were generated by coculturing osteoblasts (1×10^4 cells/well) and bone marrow cells (5×10^5 cells/well) derived from either WT or Akt1-/- littermates in a 24-multiwell plate in α-MEM containing 10% FBS, $1,25(OH)_2D_3$ (10 nM), and prostaglandin E_2 (100 nM). After 6 d, cells positively stained for TRAP containing more than three nuclei were counted as osteoclasts. In the M-CSF-dependent BMM culture system, bone marrow cells from WT or Akt1-/- mice were seeded at a density of 3×10^5 cells/well in a 24-multiwell plate and cultured in α-MEM containing 10% FBS with M-CSF (R&D Systems, 100 ng/ml) for 3 d. To generate mature osteoclasts, adherent cells (BMM) were further cultured with M-CSF (10 ng/ml) and soluble RANKL (Wako Pure Chemical, 100 ng/ml) for 3 additional days, then the number of TRAP-positive osteoclasts was counted. To determine the survival, the mature osteoclasts were deprived of M-CSF/soluble RANKL and cultured for an additional 48 h. After 8, 24, and 48 h, the number

of TRAP-positive and trypan blue-negative osteoclasts was counted.

Real-time quantitative RT-PCR

Total RNA was extracted with ISOGEN (Wako Pure Chemical), and an aliquot (1 μg) was reverse-transcribed using a PrimeScript RT reagent Kit (Takara Bio) to make single-stranded cDNA. PCR was performed on an ABI Prism 7000 Sequence Detection System (Applied Biosystems) using QuantiTect SYBR Green PCR Master Mix (QIAGEN) according to the manufacturer's instructions. All reactions were run in triplicate. After data collection, the mRNA copy number of a specific gene in total RNA was calculated with a standard curve generated with serially diluted plasmids containing PCR amplicon sequences, and normalized to the rodent total RNA (Applied Biosystems) with mouse β-actin as an internal control. Standard plasmids were synthesized with a TOPO TA Cloning Kit (Invitrogen), according to the manufacturer's instruction. Primer sequences are stated in the Supporting Protocol S1 online.

Western blot analyses

Cells were washed twice with ice-cold PBS, and proteins were extracted with M-PER (Pierce Chemical) or NE-PER (Pierce Chemical), according to the manufacturer's instructions. To detect the phosphorylation of FoxO3a, the lysates were treated with lambda protein phosphatase (New England Bio Labs). For Western blot analysis, lysates were fractionated by SDS-PAGE with 7.5–15% Tris-Glycin gradient gel or 15% Tris-Glycin gel, and transferred onto nitrocellulose membranes (BIO-RAD). After blocking with 6% milk/TBS-T, membranes were incubated with primary antibodies to pan-Akt, phospho-Akt, Akt1, Akt2, FoxO1, cleaved caspase-3, Bax, Bcl-2 (Cell Signaling Technology), FoxO3a (Upstate), Bim (BD Parmingen), Bcl-x_L (Santa Cruz Biotechnology), and β-actin (Sigma-Aldrich), followed with HRP-conjugated goat anti-mouse IgG and goat anti-rabbit IgG (Promega). Immunoreactive bands were visualized with ECL Plus (Amersham), according to the manufacturer's instructions.

Luciferase assays

MC3T3-E1 cells were plated onto 24-well plates, then subsequently transfected in triplicate with 0.1 μg of the reporter plasmid, 0.2 μg of effector plasmids, and 8 ng of pRL-TK vector (Promega) for internal control, by using FuGENE6 (Roche Diagnostics). The amount of total DNA in each well was adjusted to be equal. Details are described in Supporting Protocol S1 online. The luciferase assay was performed 48 h after transfection with a dual-luciferase reporter assay system and GloMax™ 96 Microplate Luminometer (Promega). Firefly output was normalized to Renilla output to control for transfection efficiency.

ChIP assay

ChIP assay was performed with a ChIP Assay Kit (Upstate), according to the manufacturer's instructions. PCR was performed to amplify the promoter region (−471/−67) of osteocalcin gene containing the OSE2 site which Runx2 is reported to bind [40]. Primer sequences are given in Supporting Protocol S1 online.

Statistical analyses

Means of groups were compared by ANOVA and significance of differences was determined by post-hoc testing with Bonferroni's method.

SUPPORTING INFORMATION

Figure S1 Phosphorylation and expression pattern of Akt isoforms in bone cells. (A) Time course of phosphorylated total Akt (P-Akt) and total Akt (Akt) levels determined by Western blotting in cultured mouse calvarial osteoblasts (OB) after stimulation with IGF-I or BMP-2, and in cultured bone marrow macrophages (BMM) and mature osteoclasts (OC) after stimulation with M-CSF. (B) Expressions of each Akt isoform in the cells above determined by quantitative real-time RT-PCR analysis using the same amount of template cDNA. Data are expressed as means (bars)±SEM (error bars) of the relative amount of mRNA as compared to that of Akt1.
Found at: doi:10.1371/journal.pone.0001058.s001 (0.49 MB TIF)

Figure S2 Akt1-/- mice showed growth retardation. (A) Body weight and naso-anal length of WT (+/+) and Akt1-/- littermates. Data are expressed as means (symbols)±SEM (error bars) for 4–10 mice/group. *P<0.05 vs. WT. (B) Plain X-ray images of the whole body of representative male littermates at 8 weeks of age. Bar, 1 cm.
Found at: doi:10.1371/journal.pone.0001058.s002 (1.47 MB TIF)

Figure S3 FoxO3a translocated into nucleus after serum deprivation. Time course of subcellular localization of GFP-tagged FoxO3a after serum deprivation in MC3T3-E1 cells. Bar, 20 μm.
Found at: doi:10.1371/journal.pone.0001058.s003 (2.16 MB TIF)

Figure S4 Effects of Actinomycin D, insulin, and IGF-I on Bim expression after serum deprivation. (A) Time course of Bim mRNA level determined by real-time RT-PCR after serum deprivation in cultured calvarial osteoblasts with and without Actinomycin D (1 μM). Data are normalized to those of β-actin and are expressed as means (symbols)±SEM (error bars) of the relative amount compared to time 0. (B) Time course of Bim protein level determined by Western blotting after serum deprivation in cultured calvarial osteoblasts with and without Actinomycin D (1 μM). (C) Time course of Bim mRNA level determined by real-time RT-PCR after serum deprivation in cultured calvarial osteoblasts with and without insulin (100 nM), IGF-I (10 nM), or FBS (10%). Data are normalized to those of β-actin and are expressed as means (symbols)±SEM (error bars) of the relative amount compared to time 0.
Found at: doi:10.1371/journal.pone.0001058.s004 (0.38 MB TIF)

Figure S5 Akt1 did not affect osteoblastic differentiation of immature mesenchymal cell lines. ALP staining of cultured C2C12 cells and C3H10T1/2 cells that were adenovirally transfected with GFP, $Akt1^{CA}$, or Runx2.
Found at: doi:10.1371/journal.pone.0001058.s005 (1.52 MB TIF)

Protocol S1
Found at: doi:10.1371/journal.pone.0001058.s006 (0.10 MB DOC)

ACKNOWLEDGMENTS

We are grateful to Drs. H. Katagiri and T. Asano for adenovirus expressing $Akt1^{CA}$, Dr. H. Takayanagi for luciferase reporter constructs containing osteocalcin promoter region, and Dr. R. Nishimura for adenovirus expressing Runx2.

Author Contributions

Conceived and designed the experiments: HK NK FK TA KN UC. Performed the experiments: NK FK YO SO TI TS YK YS YA. Analyzed the data: HK NK FK TI NO KH TA KN UC ST. Contributed reagents/materials/analysis tools: NH TK YO KT ST WC. Wrote the paper: HK NK.

REFERENCES

1. Harada S, Rodan GA (2003) Control of osteoblast function and regulation of bone mass. Nature 423: 349–355.
2. Boyle WJ, Simonet WS, Lacey DL (2003) Osteoclast differentiation and activation. Nature 423: 337–342.
3. Thrailkill KM, Lumpkin CK Jr, Bunn RC, Kemp SF, Fowlkes JL (2005) Is insulin an anabolic agent in bone? Dissecting the diabetic bone for clues. Am J Physiol Endocrinol Metab 289: E735–745.
4. Niu T, Rosen CJ (2005) The insulin-like growth factor-I gene and osteoporosis: a critical appraisal. Gene 361: 38–56.
5. Krishnan V, Bryant HU, Macdougald OA (2006) Regulation of bone mass by Wnt signaling. J Clin Invest 116: 1202–1209.
6. Chen D, Zhao M, Mundy GR (2004) Bone morphogenetic proteins. Growth Factors 22: 233–241.
7. Almeida M, Han L, Bellido T, Manolagas SC, Kousteni S (2005) Wnt proteins prevent apoptosis of both uncommitted osteoblast progenitors and differentiated osteoblasts by beta-catenin-dependent and -independent signaling cascades involving Src/ERK and phosphatidylinositol 3-kinase/AKT. J Biol Chem 280: 41342–41351.
8. Ghosh-Choudhury N, Abboud SL, Nishimura R, Celeste A, Mahimainathan L, et al. (2002) Requirement of BMP-2-induced phosphatidylinositol 3-kinase and Akt serine/threonine kinase in osteoblast differentiation and Smad-dependent BMP-2 gene transcription. J Biol Chem 277: 33361–33368.
9. Hanada M, Feng J, Hemmings BA (2004) Structure, regulation and function of PKB/AKT–a major therapeutic target. Biochim Biophys Acta 1697: 3–16.
10. Yang ZZ, Tschopp O, Hemmings-Mieszczak M, Feng J, Brodbeck D, et al. (2003) Protein kinase B alpha/Akt1 regulates placental development and fetal growth. J Biol Chem 278: 32124–32131.
11. Chen WS, Xu PZ, Gottlob K, Chen ML, Sokol K, et al. (2001) Growth retardation and increased apoptosis in mice with homozygous disruption of the Akt1 gene. Genes Dev 15: 2203–2208.
12. Cho H, Mu J, Kim JK, Thorvaldsen JL, Chu Q, et al. (2001) Insulin resistance and a diabetes mellitus-like syndrome in mice lacking the protein kinase Akt2 (PKB beta). Science 292: 1728–1731.
13. Garofalo RS, Orena SJ, Rafidi K, Torchia AJ, Stock JL, et al. (2003) Severe diabetes, age-dependent loss of adipose tissue, and mild growth deficiency in mice lacking Akt2/PKB beta. J Clin Invest 112: 197–208.
14. Peng XD, Xu PZ, Chen ML, Hahn-Windgassen A, Skeen J, et al. (2003) Dwarfism, impaired skin development, skeletal muscle atrophy, delayed bone development, and impeded adipogenesis in mice lacking Akt1 and Akt2. Genes Dev 17: 1352–1365.
15. Kim R (2005) Unknotting the roles of Bcl-2 and Bcl-xL in cell death. Biochem Biophys Res Commun 333: 336–343.
16. Accili D, Arden KC (2004) FoxOs at the crossroads of cellular metabolism, differentiation, and transformation. Cell 117: 421–426.
17. Tran H, Brunet A, Griffith EC, Greenberg ME (2003) The many forks in FOXO's road. Sci STKE 2003: RE5.
18. Liu X, Bruxvoort KJ, Zylstra CR, Liu J, Cichowski R, et al. (2007) Lifelong accumulation of bone in mice lacking Pten in osteoblasts. Proc Natl Acad Sci U S A 104: 2259–2264.
19. Hosaka T, Biggs WH 3rd, Tieu D, Boyer AD, Varki NM, et al. (2004) Disruption of forkhead transcription factor (FOXO) family members in mice reveals their functional diversification. Proc Natl Acad Sci U S A 101: 2975–2980.
20. Huang DC, Strasser A (2000) BH3-Only proteins-essential initiators of apoptotic cell death. Cell 103: 839–842.
21. Dijkers PF, Birkenkamp KU, Lam EW, Thomas NS, Lammers JW, et al. (2002) FKHR-L1 can act as a critical effector of cell death induced by cytokine withdrawal: protein kinase B-enhanced cell survival through maintenance of mitochondrial integrity. J Cell Biol 156: 531–542.
22. Dijkers PF, Medema RH, Lammers JW, Koenderman L, Coffer PJ (2000) Expression of the pro-apoptotic Bcl-2 family member Bim is regulated by the forkhead transcription factor FKHR-L1. Curr Biol 10: 1201–1204.
23. Gilley J, Coffer PJ, Ham J (2003) FOXO transcription factors directly activate bim gene expression and promote apoptosis in sympathetic neurons. J Cell Biol 162: 613–622.
24. Willis SN, Adams JM (2005) Life in the balance: how BH3-only proteins induce apoptosis. Curr Opin Cell Biol 17: 617–625.
25. Akiyama T, Bouillet P, Miyazaki T, Kadono Y, Chikuda H, et al. (2003) Regulation of osteoclast apoptosis by ubiquitylation of proapoptotic BH3-only Bcl-2 family member Bim. Embo J 22: 6653–6664.
26. Jilka RL, Weinstein RS, Bellido T, Parfitt AM, Manolagas SC (1998) Osteoblast programmed cell death (apoptosis): modulation by growth factors and cytokines. J Bone Miner Res 13: 793–802.
27. Fujita T, Azuma Y, Fukuyama R, Hattori Y, Yoshida C, et al. (2004) Runx2 induces osteoblast and chondrocyte differentiation and enhances their migration by coupling with PI3K-Akt signaling. J Cell Biol 166: 85–95.
28. Lee ZH, Kim HH (2003) Signal transduction by receptor activator of nuclear factor kappa B in osteoclasts. Biochem Biophys Res Commun 305: 211–214.
29. Wong BR, Besser D, Kim N, Arron JR, Vologodskaia M, et al. (1999) TRANCE, a TNF family member, activates Akt/PKB through a signaling complex involving TRAF6 and c-Src. Mol Cell 4: 1041–1049.
30. Sugatani T, Hruska KA (2005) Akt1/Akt2 and mammalian target of rapamycin/Bim play critical roles in osteoclast differentiation and survival, respectively, whereas Akt is dispensable for cell survival in isolated osteoclast precursors. J Biol Chem 280: 3583–3589.
31. Rosen CJ, Dimai HP, Vereault D, Donahue LR, Beamer WG, et al. (1997) Circulating and skeletal insulin-like growth factor-I (IGF-I) concentrations in two inbred strains of mice with different bone mineral densities. Bone 21: 217–223.
32. Liu JP, Baker J, Perkins AS, Robertson EJ, Efstratiadis A (1993) Mice carrying null mutations of the genes encoding insulin-like growth factor I (Igf-1) and type 1 IGF receptor (Igf1r). Cell 75: 59–72.
33. Canalis E, Centrella M, Burch W, McCarthy TL (1989) Insulin-like growth factor I mediates selective anabolic effects of parathyroid hormone in bone cultures. J Clin Invest 83: 60–65.
34. Yamaguchi M, Ogata N, Shinoda Y, Akune T, Kamekura S, et al. (2005) Insulin receptor substrate-1 is required for bone anabolic function of parathyroid hormone in mice. Endocrinology 146: 2620–2628.
35. Ohlsson C, Bengtsson BA, Isaksson OG, Andreassen TT, Slootweg MC (1998) Growth hormone and bone. Endocr Rev 19: 55–79.
36. Huang BK, Golden LA, Tarjan G, Madison LD, Stern PH (2000) Insulin-like growth factor I production is essential for anabolic effects of thyroid hormone in osteoblasts. J Bone Miner Res 15: 188–197.
37. Yamada T, Kawano H, Koshizuka Y, Fukuda T, Yoshimura K, et al. (2006) Carminerin contributes to chondrocyte calcification during endochondral ossification. Nat Med 12: 665–670.
38. Parfitt AM, Drezner MK, Glorieux FH, Kanis JA, Malluche H, et al. (1987) Bone histomorphometry: standardization of nomenclature, symbols, and units. Report of the ASBMR Histomorphometry Nomenclature Committee. J Bone Miner Res 2: 595–610.
39. Akune T, Ogata N, Hoshi K, Kubota N, Terauchi Y, et al. (2002) Insulin receptor substrate-2 maintains predominance of anabolic function over catabolic function of osteoblasts. J Cell Biol 159: 147–156.
40. Ducy P, Karsenty G (1995) Two distinct osteoblast-specific cis-acting elements control expression of a mouse osteocalcin gene. Mol Cell Biol 15: 1858–1869.

JOURNAL OF BONE AND MINERAL RESEARCH
Volume 22, Number 10, 2007
Published online on June 25, 2007; doi: 10.1359/JBMR.070619

Negative Feedback Loop in the Bim–Caspase-3 Axis Regulating Apoptosis and Activity of Osteoclasts

Hidetoshi Wakeyama,[1] Toru Akiyama,[1] Katsuhiko Takahashi,[2] Hitoshi Amano,[3] Yuho Kadono,[1] Masaki Nakamura,[1] Yasushi Oshima,[1] Hiroyuki Itabe,[2] Keiichi I Nakayama,[4] Keiko Nakayama,[5] Kozo Nakamura,[1] and Sakae Tanaka[1]

ABSTRACT: Proapoptotic Bcl-2 family member Bim plays an essential role in the osteoclast apoptosis and is degraded through ubiquitin/proteasome pathways in a caspase-3–dependent manner. This negative feedback loop in the Bim–caspase-3 axis is important for regulating the survival and activity of osteoclasts.

Introduction: Bim is a member of the proapoptotic Bcl-2 family and regulates the mitochondrial apoptosis pathway. Bim expression is post-translationally regulated in osteoclasts (OCs) through ubiquitin/proteasome pathways, and Bim is critical for their survival and activity.
Materials and Methods: Time-course of change in the expression of Bim in the course of OC apoptosis was examined, and the effect of various proteinase inhibitors on the degradation of Bim was analyzed. The role of caspase-3 and caspase-7 on Bim degradation was studied using RNA interference technique and *caspase-3*$^{-/-}$ mice.
Results: Bim was degraded after caspase-3 activation, which was suppressed by a caspase inhibitor and a proteasome inhibitor. Bim degradation was suppressed by gene knockdown of *caspase-3* or in *caspase-3*$^{-/-}$ OCs but not by *caspase-7* knockdown. OCs generated from *caspase-3*$^{-/-}$ bone marrow cells exhibited a shorter life span and higher bone-resorbing activity than normal OCs. Association of Bim with E3 ubiquitin ligase c-Cbl was suppressed by gene knockdown of *caspase-3* or in *caspase-3*$^{-/-}$ OCs. Actin ring formation and cathepsin K expression were promoted in *caspase-3*$^{-/-}$ OCs.
Conclusions: Caspase-3 negatively regulates Bim expression by stimulating its degradation through ubiquitin/proteasome pathways, thus creating a negative feedback loop in the Bim–caspase axis.
J Bone Miner Res 2007;22:1631–1639. Published online on June 25, 2007; doi: 10.1359/JBMR.070619

Key words: osteoclast, Bim, caspase-3, c-Cbl, degradation, apoptosis

INTRODUCTION

OSTEOCLASTS (OCs) ARE multinucleated giant cells primarily responsible for bone resorption, which rapidly die because of apoptosis in the absence of trophic factors such as macrophage-colony-stimulating factor (M-CSF) or RANKL. Bim is a member of the BH (Bcl-2 homology) 3-only family of proapoptotic proteins that regulates the mitochondrial apoptosis pathway.[1–3] Bim localizes in mitochondria, and the interaction between Bim and other Bcl-2 family proteins eventually causes oligomerization of Bax and Bak,[4] which leads to cytochrome *c* release from the mitochondria.[5] Released cytochrome *c* interacts with Apaf-1 and caspase-9 to form the apoptosome.[6] Caspase-9 in the apoptosome activates effector caspases (caspase-3 and caspase-7) that lead to apoptosis.[7] Bim is expressed in hematopoietic, epithelial, neuronal, and germ cells.[8] Experiments with knockout mice have shown that Bim is essential for apoptosis of T lymphocytes, B lymphocytes, myeloid cells, and neurons.[9–12] We previously reported that *bim*$^{-/-}$ OCs have a longer life span than *bim*$^{+/+}$ OCs, but that their bone-resorbing activity was reduced, indicating that Bim is a critical regulator of both the survival and the activation of OCs.[13]

The expression of Bim is regulated at both transcriptional and post-translational levels.[14] Previous studies have shown that Bim is regulated at the transcriptional level in hematopoietic progenitors and neurons,[11,12,15] and more recent reports revealed that the level of Bim mRNA is regulated through activation of the forkhead-like transcription factor FOXO3A (forkhead box O3A; also known as FKHRL1) in several types of cells.[16–23] On the other hand, other studies showed the post-translational regulation of Bim. Important post-translational regulation of Bim

The authors state that they have no conflicts of interest.

[1]Department of Orthopaedic Surgery, Faculty of Medicine, The University of Tokyo, Tokyo, Japan; [2]Department of Biological Chemistry, School of Pharmaceutical Sciences, Showa University, Showa, Japan; [3]Department of Pharmacology, School of Dentistry, Showa University, Showa, Japan; [4]Department of Molecular and Cellular Biology, Medical Institute of Bioregulation, Kyushu University, Kyushu, Japan; [5]Division of Developmental Genetics, Center for Translational and Advanced Animal Research on Human Diseases, Tohoku University Graduate School of Medicine, Tohoku, Japan.

includes its phosphorylation and ubiquitination. Bim is phosphorylated by extracellular-regulated kinase (ERK),[24–29] c-*jun* N-terminal kinase (JNK),[30,31] and AKT,[32] and affects the expression level or the pro-apoptotic function of Bim. Several lines of evidence have also shown that Bim is regulated through the ubiquitin/proteasome degradation process.[24,27,33,34] We previously reported that Bim expression was markedly upregulated in the course of OC apoptosis without changing its transcriptional level and was downregulated by M-CSF treatment.[13] The effect of M-CSF was abrogated by the proteasome inhibitors MG132 and lactacystin.[13] These data indicate that the expression of Bim is regulated through ubiquitin-proteasome pathways in OCs.

In this report, we further studied the mechanism of post-translational regulation of Bim in OCs.

MATERIALS AND METHODS

Reagents

Antibodies were purchased as follows: Bim, Bcl-2, and pan-ERK were from BD Biosciences Pharmingen (San Jose, CA, USA); Bcl-xL, phospho-ERK, cathepsin K, and c-Cbl were from Santa Cruz Biotechnology (Santa Cruz, CA, USA); caspase-3, cleaved-caspase-3, cleaved-caspase-7, and Bax were from Cell Signaling Technology (Beverly, MA, USA); Bak was from Upstate Cell Signaling Solutions (Lake Placid, NY, USA); β-actin was from Sigma-Aldrich; and S-tag was from Novagen (San Diego, CA, USA). A proteasome inhibitor lactacystin was purchased from BIOMOL International (Plymouth Meeting, PA, USA). Aprotinin was from Sigma-Aldrich, E-64 was from Peptide Institute (Osaka, Japan), and calpain inhibitor V was from EMD Biosciences (San Diego, CA, USA). A broad-spectrum caspase inhibitor zVAD-fmk was obtained from Sigma-Aldrich. Recombinant mouse M-CSF was from R&D Systems (Minneapolis, MN, USA), and soluble RANKL was from Wako Pure Chemical Co. (Osaka, Japan). αMEM was purchased from Gibco-BRL, Life Technologies (Rockville, MD, USA), and FBS was from Sigma.

Expression constructs and gene transduction

Small hairpin RNA (shRNA) plasmids for *caspase-3* and *caspase-7* were constructed using piGENE U6 vector (iGENE Therapeutics, Ibaraki, Japan) according to the manufacturer's protocol. The target site of *caspase-3* was 5′-AAGTAAAGACCATACATGGGA-3′ and that of *caspase-7* was 5′-AAGGCTCCTGGTTTGTGCAGG-3′. Both mU6 promoter and inserted fragment encoding a target site were subcloned from piGENE U6 vector by PCR using a set of primers 5′-CAGGAAACAGCTATGA-3′ and 5′-GTAAAACGACGGCCAG-3′. The PCR fragments were ligated into pCR-blunt II TOPO (Invitrogen) using protocols recommended by the manufacturer. The mU6 promoter and the inserted fragment were digested from TOPO vectors with *Eco*RI/*Eco*RI, and inserted into the corresponding restriction sites of pMX-bsr (kindly provided by Sunao Takeshita). To make retrovirus vectors, we transfected pMX-puro or pMX-bsr vectors into BOSC 23 packaging cell lines using FuGENE6 transfection reagent (Roche Diagnotics) and collected supernatant 24–48 h after transfection. Gene transduction to OC precursors by retrovirus and OC differentiation was performed as previously reported.[35] Empty retrovirus vector was used as a control in all the shRNA experiments, because we found no difference in Bim expression between osteoclasts infected with empty retrovirus vectors and retroviral vectors carrying shRNA-GFP (data not shown).

Real-time PCR

mRNA was isolated from cells and reverse-transcribed by the Super Script First-Strand Synthesis system for RT-PCR (Invitrogen), according to the manufacturer's protocol. Reverse-transcribed mRNA was analyzed by the ABI Prismâ 7000 Sequence Detection System (Applied Biosystems). The primers for real-time PCR to detect the bm_{EL} were 5′-CTTCCATACGACAGTCTC-3′ and 5′-AACCATTTGAGGGTGGTCTTC-3′. PCR cycles were performed 40 times as follows: 95°C for 15 s and 60°C for 60 s (two steps).

Western blotting

All extraction procedures were performed at 4°C or on ice. Cells were washed with ice-cold PBS and lysed by adding Tris-HCl, NaCl, and EDTA (TNE) buffer (1% NP-40, 10 mM of Tris-HCl [pH 7.8], 150 mM of NaCl, 1 mM of EDTA, 2 mM of Na3VO4, 10 mM of NaF, and 10 g/ml of aprotinin). The lysates were clarified by centrifugation at 15,000 rpm for 20 min. An equal amount of protein was subjected to 7.5–15% SDS-PAGE, transferred electrophoretically onto a nitrocellulose membrane, and probed sequentially with an appropriate primary antibody followed by secondary antibody coupled with horseradish peroxidase (Promega, Madison, WI, USA). Immunoreactive proteins were visualized by enhanced chemiluminescence (ECL) Western blotting detection reagents (Amersham, Arlington Heights, IL, USA) following the procedure recommended by the supplier. The blots were stripped by incubating for 20 min in stripping buffer (2% SDS, 100 mM of 2-mercaptoethanol, and 62.5 mM of Tris-HCl [pH 6.7]) at 50°C and reprobed with other antibodies.

Generation of OCs and survival/bone resorption assay

Five-week-old male ddY mice were purchased from Shizuoka Laboratories Animal Center (Shizuoka, Japan). *Caspase-3*$^{-/-}$ male mice (on a C57BL/6 genetic background) were generated as previously reported.[36] *Caspase-3*$^{+/+}$ male mice (the littermates of *caspase-3*$^{-/-}$ mice) were used as a control of *caspase-3*$^{-/-}$ mice. Bone marrow cells were obtained from femur and tibia, and bone marrow macrophages (BMMs) were generated by culturing the cells in the presence of M-CSF (100 ng/ml) for 2 days. OCs were generated by stimulating BMMs with M-CSF (10 ng/ml) and RANKL (100 ng/ml) for an additional 4–5 days or by the co-culture system established by Takahashi.[37] Survival assay was performed as follows: OCs generated in vitro were incubated for 16 h after cytokine removal. Sur-

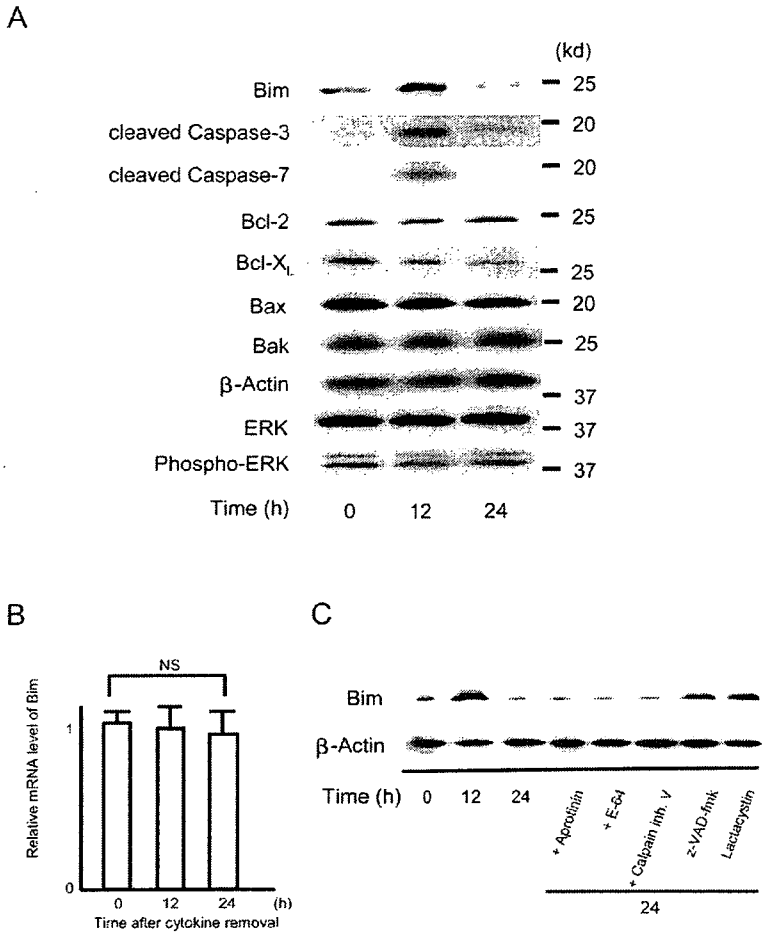

FIG. 1. Regulation of Bim in OCs. (A) The regulation of Bim in apoptotic OCs. OCs were generated from mouse BMMs generated from ddY mouse bone marrow cells by M-CSF (10 ng/ml) and RANKL (100 ng/ml) stimulation. They were incubated for an additional 24 h in the absence of cytokines. Cell lysates were obtained at each time-point (0, 12, and 24 h after cytokine removal) and subjected to Western blotting. Bim expression levels were increased 12 h after the cytokine removal and decreased 24 h after caspase-3 activation. The expression of other members of the Bcl-2 family (Bcl-2, Bcl-xL, Bax, and Bak) and activation level of ERK did not appear to change after cytokine removal. β-Actin was used as an internal control to adjust for differences in the amount of protein loaded in each lane. (B) Transcriptional regulation of *bim* in osteoclasts. Cytokine starvation did not alter *bim* mRNA level in real-time PCR. The *y*-axis indicates relative mRNA levels. (C) Effects of proteinase inhibitors on Bim degradation in OCs. Bim degradation was suppressed by a pan-caspase inhibitor zVAD-fmk or a proteasome inhibitor lactacystin, but not by aprotinin, calpain inhibitor V, or cathepsin inhibitor E64. β-Actin was used as an internal control to adjust for differences in the amount of protein loaded in each lane.

vival rate of OCs is expressed as the percentage of morphologically intact TRACP$^+$ multinucleated cells. Bone resorption assay of OCs was performed as previously reported.[38] In brief, the cells were cultured on dentine slices for 16 h, and the resorption pits were visualized by staining with 1% toluidine blue. The resorbed area was measured using an image analysis system (SYSTEM SUPPLY) linked to a light microscope (Nikon). The actin rings of OCs were visualized by staining with rhodamine-phalloidin (Molecular Probes).

In vitro cleavage assay

Mouse recombinant caspase-3 was obtained from Calbiochem (San Diego, CA, USA). Recombinant Bim_{EL} and ICA_{DL} (inhibitor of caspase-3–activated DNAse; also known as DFF45 [DNA Fragmentation Factor 45]; positive control) were obtained using the TNT T7 Quick Coupled Transcription/Translation System (Promega). In brief, both bim_{EL} and ICA_{DL} encoding genes were inserted into the *Eco*RI/*Not*I sites and *Bam*HI/*Bam*HI sites of pCITE-vector (Novagen), respectively. These vectors were used for translation according to the manufacturer's protocol. Obtained S-tagged recombinant proteins were immunoprecipitated by anti-S-tag antibody and incubated with sufficient amount of recombinant caspase-3 as previously reported.[39]

Statistical analysis

Each series of experiments was repeated at least three times. The results obtained from a typical experiment were expressed as means ± SD. Significant differences were determined using factorial ANOVA.

RESULTS

Bim expression level is downregulated by caspase-3 in OCs

To study the molecular mechanisms underlying the degradation of Bim in detail, we studied the protein dynamics of Bim in OCs. OCs generated from mouse bone marrow cells in the presence of recombinant human M-CSF (10 ng/ml) and soluble RANKL (100 ng/ml) underwent cell death within 48 h after removal of these cytokines. As we previously reported, the protein level of Bim increased after 12 h of the cytokine removal. However, its level was decreased again after 24 h (Fig. 1A), whereas its mRNA

level did not alter (Fig. 1B). The expression of other Bcl-2 family members did not appear to change (Fig. 1A).

We next examined the effect of various proteinase inhibitors on the degradation of Bim in OCs. As shown in Fig. 1C, a pan-caspase inhibitor zVAD-fmk and a proteasome inhibitor lactacystin but no other proteinase inhibitors maintained Bim at high levels after 24 h of the cytokine removal (Fig. 1C). These results led us to speculate that caspase activation is important for the degradation process of Bim.

Retrovirus vector–mediated shRNA/caspase-3 transduction reduced the level of caspase-3, and its activation was reduced even 24 h after the cytokine removal, whereas caspase-7 activation was observed at a similar level as in the control OCs (Fig. 2A). In contrast, knockdown of *caspase-7* did not affect the degradation of Bim in OCs, although shRNA/caspase-7 efficiently reduced the expression level of caspase-7 (Fig. 2B). To further confirm the role of caspase-3 on Bim degradation in OCs, we generated OCs from *caspase-3*–deficient mouse bone marrow cells. The degradation of Bim was reduced in *caspase-3*$^{-/-}$ OCs, and a high level of Bim expression was maintained 24 h after cytokine withdrawal (Fig. 2C). Caspase-7 activation was observed in *caspase-3*$^{-/-}$ OCs at a comparable level as control OCs. These results suggest that caspase-3 is critically involved in the degradation of Bim in OCs.

Caspase-3 regulates the association of Bim with c-Cbl

To analyze the direct effect of caspase-3 on the degradation of Bim, we generated recombinant Bim and ICAD and incubated them with active caspase-3. After 25-h incubation, cleavage of ICAD was clearly observed as shown in the left panels of Fig. 3A, whereas the degradation of Bim was not observed, as shown in the right panels (Fig. 3A), indicating that caspase-3 activation indirectly induces the degradation of Bim. We previously reported that ubiquitin E3 ligase c-Cbl is involved in the ubiquitination and the degradation of Bim in OCs.[13] We therefore examined whether the association between c-Cbl and Bim is affected by caspase-3. Stable association of Bim and c-Cbl was detected in OCs, and this association was suppressed by caspase-3 knockdown by shRNA/caspase-3 (Fig. 3B, left). OCs were generated from bone marrow cells obtained from *caspase-3*$^{-/-}$ mice, and the association of Bim and c-Cbl was examined by immunoprecipitation. As shown in Fig. 3B, their association was reduced in *caspase-3*$^{-/-}$ OCs. These results suggest that caspase-3 promotes the association between Bim and c-Cbl, which may induce the degradation of Bim through ubiquitin/proteasome pathways after caspase-3 activation.

Caspase-3 regulates survival and activation of OCs

We next examined the effect of *caspase-3* deficiency on the survival and the activation of OCs. There was no significant difference in OC differentiation between bone marrow cells from *caspase-3*$^{-/-}$ mice and their normal littermates (*caspase-3*$^{+/+}$ mice) (Fig. 4C). In contrast, the survival of OCs transduced with shRNA/caspase-3 exhibited a shorter lifespan and increased bone-resorbing activity than

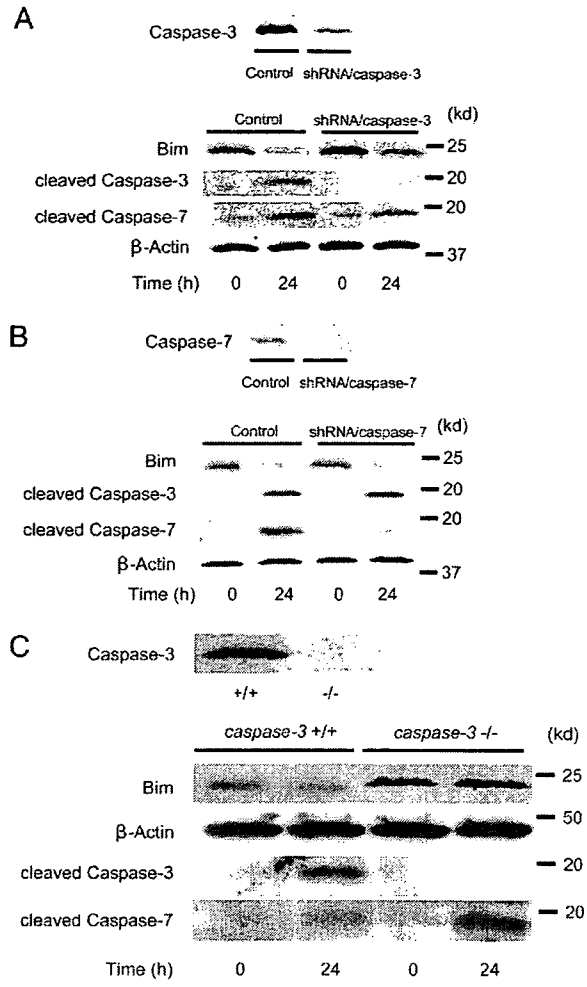

FIG. 2. Involvement of caspase-3 in Bim degradation in OCs. Effects of shRNA/caspase-3 (A) and shRNA/caspases-7 (B) on Bim degradation in OCs. (A; top) ShRNA/caspase-3 was transduced to BMMs by retroviral infection, and OCs were generated from these cells by M-CSF and RANKL stimuli. Cell lysates were obtained at each time-point (0, 12, and 24 h after cytokine removal) and subjected to Western blotting. Caspase-3 was downregulated in the cells compared with control OCs. (Bottom) In shRNA/caspase-3–transduced OCs, activation of caspase-7 but not caspase-3 was observed, and the Bim expression level was higher than control OCs both at the basal level and 24 h after cytokine deprivation. β-Actin was used as an internal control to adjust for differences in the amount of protein loaded in each lane. Bim level was reduced to 0.36-fold after 24 h in control OCs compared with 0.71-fold in shRNA/caspase-3–transduced cells. (B; top) Retrovirus-mediated shRNA/caspases-7 transduction efficiently downregulated caspase-7 expression in OCs. (Bottom) Activation of caspase-7 was markedly reduced in shRNA/caspases-7–transduced OCs, whereas caspase-3 activation was similarly observed. Bim degradation was not affected by shRNA/caspases-7 transduction. (C) Bim expression in *caspases-3*$^{-/-}$ OCs. (Top) Western blotting of caspase-3 in OCs generated from bone marrow cells of *caspases-3*$^{-/-}$ mice or their normal littermates (C57BL/6 genetic background). (Bottom) Bim degradation was not observed 24 h after the cytokine removal in *caspase-3*$^{-/-}$ OCs. Caspase-7 activation was observed in *caspase-3*$^{-/-}$ OCs at a comparable level as control OCs. β-Actin was used as an internal control to adjust for differences in the amount of protein loaded in each lane.

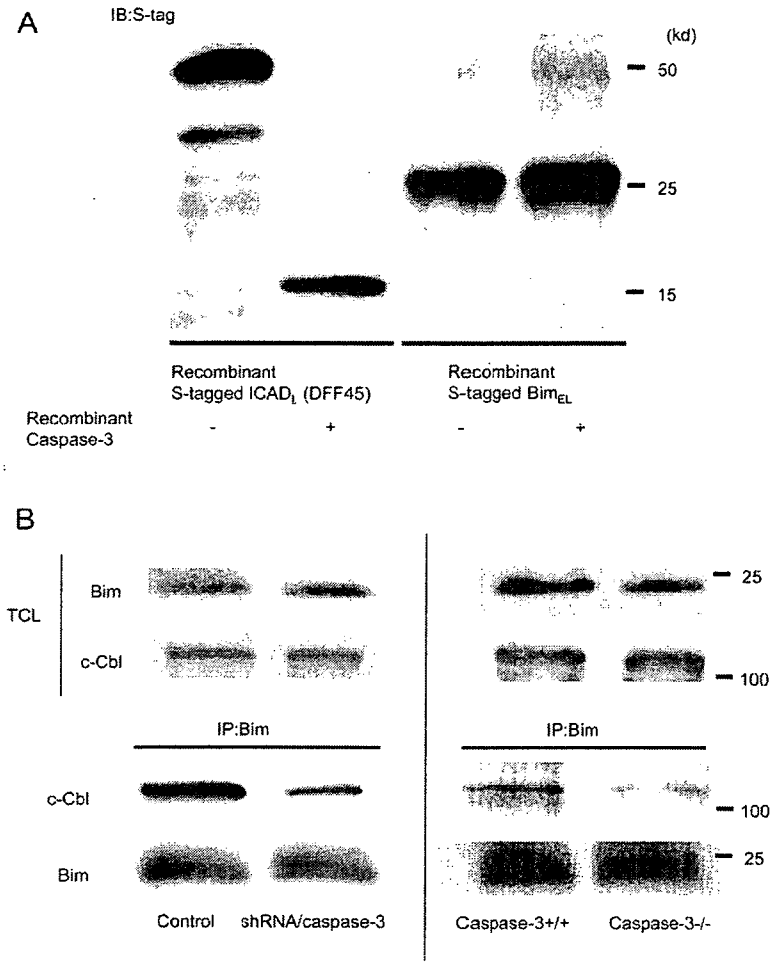

FIG. 3. Effects of caspase-3 on Bim association with c-Cbl. (A) Effects of caspase-3 on Bim in vitro. Both S-tagged recombinant Bim_{EL} and S-tagged recombinant ICA_{DL} were incubated with or without sufficient amount of recombinant caspase-3 and analyzed by Western blotting using anti-S-tag antibody. ICA_{DL} blots are shown as a positive control of caspase-3 activity. Recombinant ICA_{DL} was cleaved to a smaller protein by recombinant caspase-3 as previously reported. Recombinant Bim_{EL} was not cleaved/degraded by recombinant caspase-3. (B) Association of Bim with c-Cbl in OCs. (Left) Bim was immunoprecipitated from cell lysates of control OCs or OCs transduced by shRNA/caspases-3 and Western-blotted with anti-c-Cbl antibody. Although the expression levels of Bim and c-Cbl were not different (top, TCL: total cell lysates), the amount of c-Cbl co-immunoprecipitated with Bim was significantly decreased in shRNA/caspase-3–transduced OCs compared with control OCs. (Right) Immunoprecipitation by Bim was performed from cell lysates of *caspase-3*$^{+/+}$ and *caspase-3*$^{-/-}$ OCs (C57BL/6 genetic background). The amount of c-Cbl associated with Bim was significantly reduced in *caspase-3*$^{-/-}$ OCs. No difference in the expression level of Bim or c-Cbl level was observed between *caspase-3*$^{+/+}$ and *caspase-3*$^{-/-}$ OCs.

the control OCs, whereas gene knockdown of *caspase-7* by shRNA did not appear to change their survival or activity compared with control OCs (Figs. 4A and 4B). These observations were also confirmed by the experiments using *caspase-3*$^{-/-}$ mouse cells, and OCs generated from *caspase-3*$^{-/-}$ bone marrow cells showed a shorter lifespan and a higher bone-resorbing activity than the OCs generated from normal littermates (*caspase-3*$^{+/+}$) (Fig. 4D). These results were consistent with the in vivo observations that the number of OCs is reduced in the bone tissues of *caspase-3*$^{-/-}$ mice (data not shown), which was already reported by other groups.[40] We finally examined the actin ring formation and the expression level of cathepsin K of *caspase-3*$^{+/+}$ and *caspase-3*$^{-/-}$ OCs. Proportion of OCs that developed actin ring was higher (Fig. 4E), and the expression level of cathepsin K (Fig. 4F) was higher in *caspase-3*$^{-/-}$ OCs compared with *caspase-3*$^{+/+}$ OCs.

DISCUSSION

We previously reported that the pro-apoptotic Bcl-2 family member Bim is a key regulator of the survival and the activity of OCs.[13] Trophic factors such as M-CSF and RANKL maintained the protein level of Bim at low levels by inducing its ubiquitination, which is at least partly mediated by ERK pathways and an E3 ubiquitin ligase c-Cbl.[13] Removal of the cytokines increases the protein levels of Bim by reducing its ubiquitination, which leads to cytochrome *c* release from mitochondria and activation of caspase cascades. However, 24 h after cytokine removal, the protein level of Bim was decreased again without change in its transcriptional levels (Figs. 1A and 1B). ERK does not seem to be involved in this process because no change in ERK activity was observed (Fig. 1A). Neither was this caused by the general protein degradation during the cell death process because the expression of other members of the Bcl-2 family did not seem to have altered at this time-point (Fig. 1A). It is possible that the levels of other Bcl-2 family members did not change because their protein half-lives are longer than that of Bim. However, at least we can argue that Bim is degraded much faster than other Bcl-2 family members in OCs.

Bim degradation was suppressed by a pan-caspase inhibitor zVAD-fmk (Fig. 1C), and degradation of Bim was suppressed by *caspase-3* gene knockdown but not by *caspase-7*

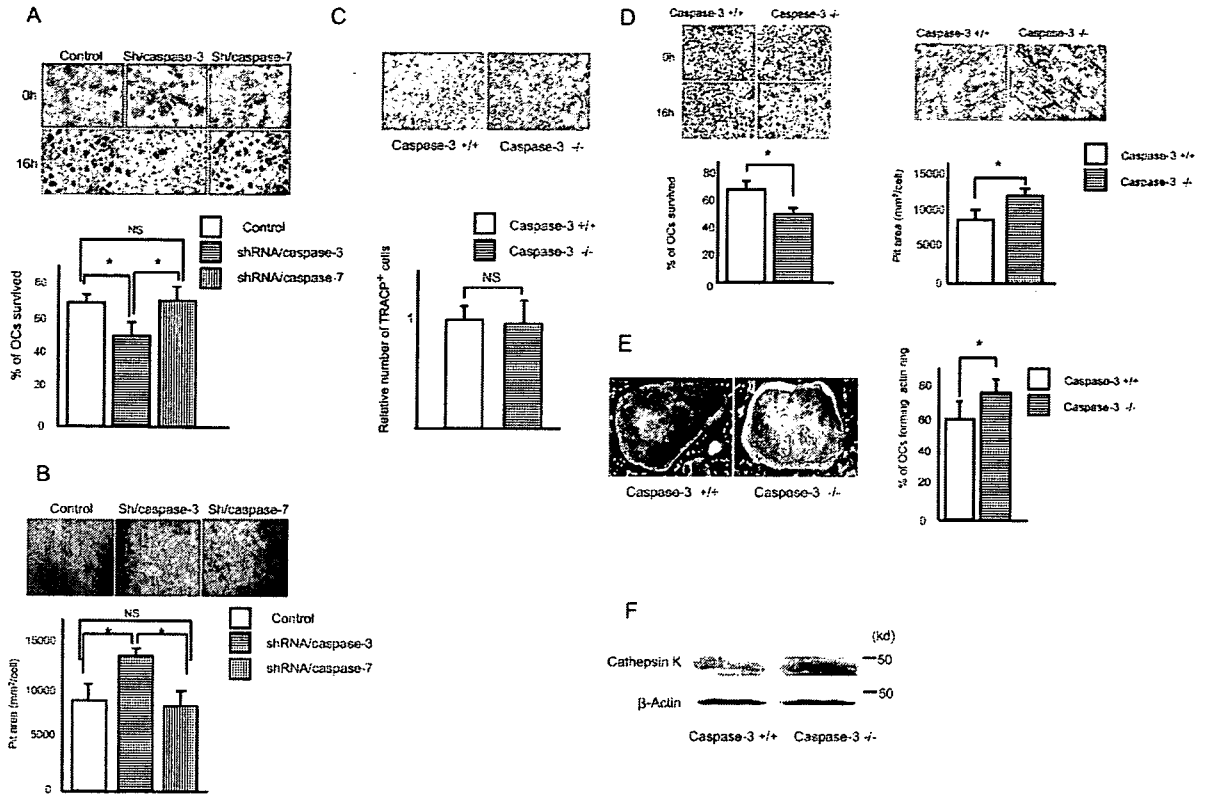

FIG. 4. Effects of caspase-3 and caspase-7 on the survival and activation of OCs. (A) ShRNA/caspase-3–transduced OCs exhibited a shorter lifespan than control OCs. OCs were generated from mouse bone marrow cells (ddY genetic background) with or without retrovirus-mediated shRNA/caspases-3 or shRNA/caspase-7 transduction and incubated for 16 h after cytokine deprivation. The top panels show representative TRACP staining of control OCs (left), shRNA/caspase-3–transduced OCs (middle), and shRNA/caspase-7–transduced OCs (right) at the starting time-point and 16 h after incubation, respectively. The bottom panel shows the survival rate after 16 h. OCs transduced with shRNA/caspase-3 exhibited a significantly reduced level of survival than control cells, whereas shRNA/caspase-7 transduction did not affect their survival. Error bars represent SD. *Significantly different, $p < 0.01$; NS, not statistically significant difference. (B) ShRNA/caspase-3–transduced OCs exhibited increased bone-resorbing activity than control OCs. The top panels show representative pictures of resorption pits created by control OCs (left), shRNA/caspase-3–transduced OCs (middle), and shRNA/caspase-7–transduced OCs (right) stained by toluidine blue. The bottom panel shows pit area per cell (μm^2/cell) formed on dentine slices. OCs transduced with shRNA/caspase-3 exhibited significantly higher bone-resorbing activity than control OCs, whereas shRNA/casapse-7 transduction did not affect it. Error bars represent SD. *Significantly different, $p < 0.01$; NS, not statistically significant difference. (C) Caspase-3 deficiency does not affect OC differentiation in vitro. Bone marrow cells were obtained from femur and tibia of *caspase-3*$^{-/-}$ mice and their normal littermates (C57BL/6 genetic background), and BMMs were generated by culturing the cells in the presence of M-CSF (100 ng/ml) for 2 days. OCs were generated by stimulating BMMs with M-CSF (10 ng/ml) and RANKL (100 ng/ml) for an additional 4 days, and the number of TRACP$^+$ cells per well was counted. The top panels show the representative TRACP staining of *caspase-3*$^{-/-}$ OCs (right) and control OCs (left). The *y*-axis represents the relative number of TRACP$^+$ cells. NS, not statistically significant difference. (D) *Caspase-3*$^{-/-}$ OCs exhibited a shorter life span and a higher bone-resorbing activity than *caspase-3*$^{+/+}$ OCs. OCs were generated from bone marrow cells of *caspase-3*$^{-/-}$ mice or their normal littermates (C57BL/6 genetic background) and subjected to the survival assay and bone resorption assay. The top left panels show representative TRACP staining of *caspase-3*$^{-/-}$ OCs (right) and control OCs (left) at the starting point and 16 h after incubation, respectively. The top right panels show the representative resorption pits created by *caspase-3*$^{-/-}$ OCs (right) and control OCs (left) stained by toluidine blue. Survival rate after 16-h incubation (bottom left) and pit area per cell (μm^2/cell) formed on dentine slices (bottom right) are shown. *Caspase-3*$^{-/-}$ OCs exhibited a significantly lower survival rate and a higher bone-resorbing activity than control OCs. Error bars represent SD. *Significantly different, $p < 0.01$. (E) The proportion of OCs with actin ring structure is higher under *caspase-3*$^{-/-}$ background. OCs derived from *caspase-3*$^{+/+}$ and $^{-/-}$ mouse bone marrow cells by M-CSF and RANKL stimulation were stained with rhodamine-phalloidin. The top panels show the typical actin ring staining of *caspase-3*$^{+/+}$ OCs (left panels) and *caspase-3*$^{-/-}$ OCs (right panels), and the bottom panels present higher magnification view (bars: 100 μm). The bottom graph shows the ratio of OCs forming clear actin ring structure to the total number of OCs. *Significantly different, $p < 0.01$. (F) *Caspase-3*$^{-/-}$ OCs exhibit higher expression level of cathepsin K than control OCs. Cell lysates obtained from OCs derived from *caspase-3*$^{+/+}$ and $^{-/-}$ mouse bone marrow cells were subjected to Western blotting. Expression level of cathepsin K in *caspase-3*$^{-/-}$ OCs was higher than that in *caspase-3*$^{+/+}$ OCs. β-Actin was used as an internal control of the amount of protein loaded in each lane.

knockdown (Figs. 2A and 2B). The degradation of Bim was also reduced in OCs generated from *caspase-3*$^{-/-}$ mouse bone marrow cells (Fig. 2C). These results suggest that caspase-3 but not caspase-7 is involved in the degradation of Bim in OCs.

The mechanism of how caspase-3 activation induces the

degradation of Bim remains unclear. A previous study has shown that caspase-3 cleaves Bim at the N terminus, and the unphosphorylated Bim was sequestered to microtubules by means of a direct interaction with tubulin, the phosphorylated protein was released from microtubules. The N-terminally cleaved Bim interacts with Bcl-2 and induces apoptosis more efficiently than uncleaved Bim, indicating that Bim cleavage by caspase triggers a positive feedback amplification of apoptotic signaling.[41] However, we found that caspase-3 itself was unable to degrade Bim directly, even when active caspase-3 was incubated with recombinant Bim in vitro (Fig. 3A), indicating that caspase-3 indirectly stimulates Bim degradation. Bim degradation was suppressed by a proteasome inhibitor lactacystin (Fig. 1C). Bim is stably associated with ubiquitin E3 ligase c-Cbl in OCs, and this association was suppressed by shRNA/caspase-3 introduction or in *caspase-3*$^{-/-}$ OCs (Fig. 3B). These results suggest that caspase-3 is required for the association of Bim with c-Cbl, which may be involved in the degradation of Bim. Although c-Cbl is stably associated with Bim in OCs, the degradation of Bim requires caspase-3 activation. Therefore, partial cleavage of Bim or c-Cbl by caspase-3 may activate the degradation of Bim through ubiquitin/proteasome pathways (Fig. 5). This does not exclude the possibility that other E3 ubiquitin ligases are involved in the degradation process, and further studies are necessary.

In an attempt to elucidate the role of degradation of Bim by caspase-3 in OCs, we analyzed the survival and bone-resorbing activity of OCs in which the expression of caspase-3 is reduced by shRNA/caspases-3 introduction or OCs generated from *caspase-3*–deficient animals. Although caspase-3 is known to be an executor of apoptosis in various types of cells, the apoptosis of OCs was instead promoted by caspase-3 deficiency, and they exhibited an increased bone-resorbing activity compared with control OCs (Figs. 4A, 4B, and 4D). Consistent with these in vitro observations, previous studies showed that the number of OCs in *caspases-3*$^{-/-}$ mice was reduced compared with that in their normal littermates, although *caspases-3*$^{-/-}$ mice showed osteopenia.[40] These results suggest that caspase-3 activation regulates both survival and activation of OCs by regulating Bim degradation. Although it remains to be clarified how Bim stimulates bone-resorbing activity of OCs still remains unclear, we found that the actin ring formation and the expression of cathepsin K were increased in *caspase-3*$^{-/-}$ OCs compared with *caspase-3*$^{+/+}$ OCs (Figs. 4E and 4F). This may explain the promoted bone-resorbing activity of *caspase-3*$^{-/-}$ OCs to some extent, although the mechanism of how Bim controls actin ring formation and cathepsin K expression needs further study.

Recently, Szymczyk et al.[42] reported that caspase-3 activation is required for osteoclast differentiation. However, we failed to show any difference in OC differentiation between bone marrow cells from *caspase-3*$^{-/-}$ mice and their normal littermates (Fig. 4C). The reason for this discrepancy remains unknown, and further study will be needed to clarify the role of caspase-3 on the differentiation process of OCs. Further insights into the physiological and pathological role of Bim and caspase-3 in bone tissue will be obtained by generating *bim/caspase-3* doubly deficient mice.

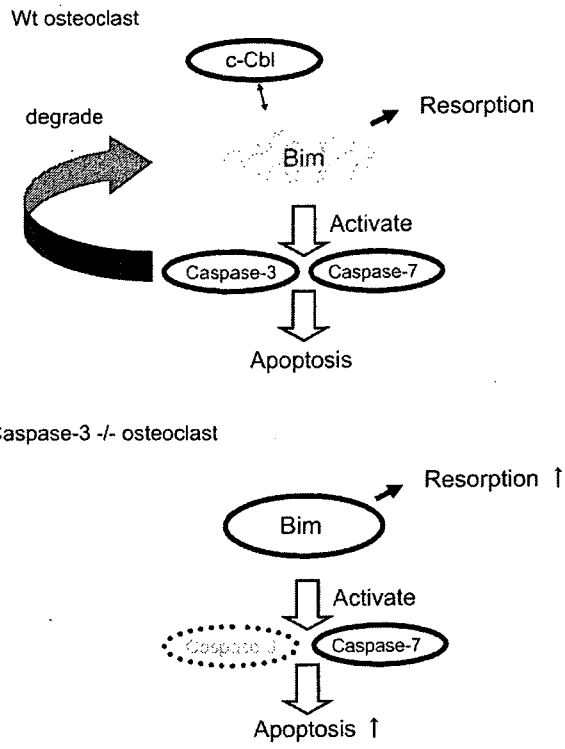

FIG. 5. Schematic representation of the mechanism of apoptosis and activation of OCs through the Bim–caspase-3 axis. (Top) Under physiological conditions, Bim activates caspase-3 through the mitochondrial apoptosis pathway that finally causes the degradation of Bim by promoting the association between Bim and c-Cbl (negative feedback loop). (Bottom) Caspase-3 deficiency suppresses the degradation of Bim, which promotes the apoptosis of OCs, probably through caspase-7 pathways and stimulates their bone-resorbing activity.

Gene knockdown of *caspase-7* neither affected the degradation process of Bim (Fig. 2B) nor the survival and activity of OCs (Figs. 4A and 4B), suggesting a distinct role for caspase-3 and caspase-7 in OCs. Chandler et al.[43] reported a distinct subcellular localization of the effector caspase-3 and caspase-7 in anti-Fas antibody-induced hepatocyte apoptosis, and several studies showed the distinct substrate specificity between these two molecules. The subcellular localization of these caspases in OCs has not been examined in detail, and further study is needed. On the basis of our findings, we speculate that upregulation of Bim induces activation of both caspase-3 and caspase-7 and that caspase-3 is important for the degradation of Bim and caspase-7 is important for the pro-apoptotic function of Bim (Fig. 5).

The physiological importance of this negative feedback loop from caspase-3 to Bim is not understood. This can be a sophisticated system regulating the timing and intensity of cell death. Osteoclasts under apoptotic condition may control Bim expression level negatively, and thereby prevents rapid and excessive cell death. We found that Bim regulates

not only apoptosis of osteoclasts but also their bone-resorbing activity. Therefore, the negative regulation of Bim may control the physiological bone resorption by OCs.

In conclusion, Bim regulates both the survival and the activity of OCs, and post-translational regulation of Bim through a negative feedback loop in the caspase-3/Bim axis plays a critical role in the regulation.

ACKNOWLEDGMENTS

The authors thank R Yamaguchi (Department of Orthopaedic Surgery, The University of Tokyo), who provided expert technical assistance. This work was supported in part by Grants-in-Aid from the Ministry of Education, Culture, Sports, Science, and Technology of Japan, Japan Aerospace Exploration Agency (JAXA), and Health Science research grants from the Ministry of Health, Labor, and Welfare of Japan to ST.

REFERENCES

1. O'Connor L, Strasser A, O'Reilly LA, Hausmann G, Adams JM, Cory S, Huang DC 1998 Bim: A novel member of the Bcl-2 family that promotes apoptosis. EMBO J **17**:384–395.
2. Puthalakath H, Huang DC, O'Reilly LA, King SM, Strasser A 1999 The proapoptotic activity of the Bcl-2 family member Bim is regulated by interaction with the dynein motor complex. Mol Cell **3**:287–296.
3. Gross A, McDonnell JM, Korsmeyer SJ 1999 BCL-2 family members and the mitochondria in apoptosis. Genes Dev **13**:1899–1911.
4. Korsmeyer SJ, Wei MC, Saito M, Weiler S, Oh KJ, Schlesinger PH 2000 Pro-apoptotic cascade activates BID, which oligomerizes BAK or BAX into pores that result in the release of cytochrome c. Cell Death Differ **7**:1166–1173.
5. Adrain C, Creagh EM, Martin SJ 2001 Apoptosis-associated release of Smac/DIABLO from mitochondria requires active caspases and is blocked by Bcl-2. EMBO J **20**:6627–6636.
6. Acehan D, Jiang X, Morgan DG, Heuser JE, Wang X, Akey CW 2002 Three-dimensional structure of the apoptosome: Implications for assembly, procaspase-9 binding, and activation. Mol Cell **9**:423–432.
7. Siegel RM 2006 Caspases at the crossroads of immune-cell life and death. Nat Rev Immunol **6**:308–317.
8. O'Reilly LA, Cullen L, Visvader J, Lindeman GJ, Print C, Bath ML, Huang DC, Strasser A 2000 The proapoptotic BH3-only protein bim is expressed in hematopoietic, epithelial, neuronal, and germ cells. Am J Pathol **157**:449–461.
9. Bouillet P, Metcalf D, Huang DC, Tarlinton DM, Kay TW, Kontgen F, Adams JM, Strasser A 1999 Proapoptotic Bcl-2 relative Bim required for certain apoptotic responses, leukocyte homeostasis, and to preclude autoimmunity. Science **286**:1735–1738.
10. Bouillet P, Purton JF, Godfrey DI, Zhang LC, Coultas L, Puthalakath H, Pellegrini M, Cory S, Adams JM, Strasser A 2002 BH3-only Bcl-2 family member Bim is required for apoptosis of autoreactive thymocytes. Nature **415**:922–926.
11. Putcha GV, Moulder KL, Golden JP, Bouillet P, Adams JA, Strasser A, Johnson EM 2001 Induction of BIM, a proapoptotic BH3-only BCL-2 family member, is critical for neuronal apoptosis. Neuron **29**:615–628.
12. Whitfield J, Neame SJ, Paquet L, Bernard O, Ham J 2001 Dominant-negative c-Jun promotes neuronal survival by reducing BIM expression and inhibiting mitochondrial cytochrome c release. Neuron **29**:629–643.
13. Akiyama T, Bouillet P, Miyazaki T, Kadono Y, Chikuda H, Chung UI, Fukuda A, Hikita A, Seto H, Okada T, Inaba T, Sanjay A, Baron R, Kawaguchi H, Oda H, Nakamura K, Strasser A, Tanaka S 2003 Regulation of osteoclast apoptosis by ubiquitylation of proapoptotic BH3-only Bcl-2 family member Bim. EMBO J **22**:6653–6664.
14. Huang DC, Strasser A 2000 BH3-Only proteins-essential initiators of apoptotic cell death. Cell **103**:839–842.
15. Shinjyo T, Kuribara R, Inukai T, Hosoi H, Kinoshita T, Miyajima A, Houghton PJ, Look AT, Ozawa K, Inaba T 2001 Downregulation of Bim, a proapoptotic relative of Bcl-2, is a pivotal step in cytokine-initiated survival signaling in murine hematopoietic progenitors. Mol Cell Biol **21**:854–864.
16. Essafi A, Fernandez de Mattos S, Hassen YA, Soeiro I, Mufti GJ, Thomas NS, Medema RH, Lam EW 2005 Direct transcriptional regulation of Bim by FoxO3a mediates STI571-induced apoptosis in Bcr-Abl-expressing cells. Oncogene **24**:2317–2329.
17. Gilley J, Coffer PJ, Ham J 2003 FOXO transcription factors directly activate bim gene expression and promote apoptosis in sympathetic neurons. J Cell Biol **162**:613–622.
18. Moller C, Alfredsson J, Engstrom M, Wootz H, Xiang Z, Lennartsson J, Jonsson JI, Nilsson G 2005 Stem cell factor promotes mast cell survival via inactivation of FOXO3a-mediated transcriptional induction and MEK-regulated phosphorylation of the proapoptotic protein Bim. Blood **106**:1330–1336.
19. Rosas M, Birkenkamp KU, Lammers JW, Koenderman L, Coffer PJ 2005 Cytokine mediated suppression of TF-1 apoptosis requires PI3K activation and inhibition of Bim expression. FEBS Lett **579**:191–198.
20. Stahl M, Dijkers PF, Kops GJ, Lens SM, Coffer PJ, Burgering BM, Medema RH 2002 The forkhead transcription factor FoxO regulates transcription of p27Kip1 and Bim in response to IL-2. J Immunol **168**:5024–5031.
21. Sunters A, Fernandez de Mattos S, Stahl M, Brosens JJ, Zoumpoulidou G, Saunders CA, Coffer PJ, Medema RH, Coombes RC, Lam EW 2003 FoxO3a transcriptional regulation of Bim controls apoptosis in paclitaxel-treated breast cancer cell lines. J Biol Chem **278**:49795–49805.
22. Urbich C, Knau A, Fichtlscherer S, Walter DH, Bruhl T, Potente M, Hofmann WK, de Vos S, Zeiher AM, Dimmeler S 2005 FOXO-dependent expression of the proapoptotic protein Bim: Pivotal role for apoptosis signaling in endothelial progenitor cells. FASEB J **19**:974–976.
23. Dijkers PF, Birkenkamp KU, Lam EW, Thomas NS, Lammers JW, Koenderman L, Coffer PJ 2002 FKHR-L1 can act as a critical effector of cell death induced by cytokine withdrawal: Protein kinase B-enhanced cell survival through maintenance of mitochondrial integrity. J Cell Biol **156**:531–542.
24. Ley R, Balmanno K, Hadfield K, Weston C, Cook SJ 2003 Activation of the ERK1/2 signaling pathway promotes phosphorylation and proteasome-dependent degradation of the BH3-only protein, Bim. J Biol Chem **278**:18811–18816.
25. Ley R, Ewings KE, Hadfield K, Cook SJ 2005 Regulatory phosphorylation of Bim: Sorting out the ERK from the JNK. Cell Death Differ **12**:1008–1014.
26. Ley R, Ewings KE, Hadfield K, Howes E, Balmanno K, Cook SJ 2004 Extracellular signal-regulated kinases 1/2 are serum-stimulated "Bim(EL) kinases" that bind to the BH3-only protein Bim(EL) causing its phosphorylation and turnover. J Biol Chem **279**:8837–8847.
27. Luciano F, Jacquel A, Colosetti P, Herrant M, Cagnol S, Pages G, Auberger P 2003 Phosphorylation of Bim-EL by Erk1/2 on serine 69 promotes its degradation via the proteasome pathway and regulates its proapoptotic function. Oncogene **22**:6785–6793.
28. Harada H, Quearry B, Ruiz-Vela A, Korsmeyer SJ 2004 Survival factor-induced extracellular signal-regulated kinase phosphorylates BIM, inhibiting its association with BAX and proapoptotic activity. Proc Natl Acad Sci USA **101**:15313–15317.
29. Biswas SC, Greene LA 2002 Nerve growth factor (NGF) down-regulates the Bcl-2 homology 3 (BH3) domain-only protein Bim and suppresses its proapoptotic activity by phosphorylation. J Biol Chem **277**:49511–49516.
30. Lei K, Davis RJ 2003 JNK phosphorylation of Bim-related

members of the Bcl2 family induces Bax-dependent apoptosis. Proc Natl Acad Sci USA **100**:2432–2437.
31. Putcha GV, Le S, Frank S, Besirli CG, Clark K, Chu B, Alix S, Youle RJ, LaMarche A, Maroney AC, Johnson EM Jr 2003 JNK-mediated BIM phosphorylation potentiates BAX-dependent apoptosis. Neuron **38**:899–914.
32. Qi XJ, Wildey GM, Howe PH 2006 Evidence that Ser87 of BimEL is phosphorylated by Akt and regulates BimEL apoptotic function. J Biol Chem **281**:813–823.
33. Styles NA, Zhu W, Li X 2005 Phosphorylation and down-regulation of Bim by muscarinic cholinergic receptor activation via protein kinase C. Neurochem Int **47**:519–527.
34. Meller R, Cameron JA, Torrey DJ, Clayton CE, Ordonez AN, Henshall DC, Minami M, Schindler CK, Saugstad JA, Simon RP 2006 Rapid degradation of Bim by the ubiquitin-proteasome pathway mediates short-term ischemic tolerance in cultured neurons. J Biol Chem **281**:7429–7436.
35. Kadono Y, Okada F, Perchonock C, Jang HD, Lee SY, Kim N, Choi Y 2005 Strength of TRAF6 signalling determines osteoclastogenesis. EMBO Rep **6**:171–176.
36. Morishita H, Makishima T, Kaneko C, Lee YS, Segil N, Takahashi K, Kuraoka A, Nakagawa T, Nabekura J, Nakayama K, Nakayama KI 2001 Deafness due to degeneration of cochlear neurons in caspase-3-deficient mice. Biochem Biophys Res Commun **284**:142–149.
37. Takahashi N, Akatsu T, Udagawa N, Sasaki T, Yamaguchi A, Moseley JM, Martin TJ, Suda T 1988 Osteoblastic cells are involved in osteoclast formation. Endocrinology **123**:2600–2602.
38. Miyazaki T, Katagiri H, Kanegae Y, Takayanagi H, Sawada Y, Yamamoto A, Pando MP, Asano T, Verma IM, Oda H, Nakamura K, Tanaka S 2000 Reciprocal role of ERK and NF-kappaB pathways in survival and activation of osteoclasts. J Cell Biol **148**:333–342.
39. Sakahira H, Enari M, Nagata S 1998 Cleavage of CAD inhibitor in CAD activation and DNA degradation during apoptosis. Nature **391**:96–99.
40. Miura M, Chen XD, Allen MR, Bi Y, Gronthos S, Seo BM, Lakhani S, Flavell RA, Feng XH, Robey PG, Young M, Shi S 2004 A crucial role of caspase-3 in osteogenic differentiation of bone marrow stromal stem cells. J Clin Invest **114**:1704–1713.
41. Chen D, Zhou Q 2004 Caspase cleavage of BimEL triggers a positive feedback amplification of apoptotic signaling. Proc Natl Acad Sci USA **101**:1235–1240.
42. Szymczyk KH, Freeman TA, Adams CS, Srinivas V, Steinbeck MJ 2006 Active caspase-3 is required for osteoclast differentiation. J Cell Physiol **209**:836–844.
43. Chandler JM, Cohen GM, MacFarlane M 1998 Different subcellular distribution of caspase-3 and caspase-7 following Fas-induced apoptosis in mouse liver. J Biol Chem **273**:10815–10818.

Address reprint requests to:
Sakae Tanaka, Md, PhD
Department of Orthopaedic Surgery
Faculty of Medicine,
The University of Tokyo
7-3-1 Hongo, Bunkyo-ku
Tokyo 113-0033, Japan
E-mail: tanakas-ort@h.u-tokyo.ac.jp

Received in original form December 22, 2006; revised form February 23, 2007; accepted June 18, 2007.

アディポサイトカイン

大島和也*　下村伊一郎*,**
OSHIMA Kazuya, SHIMOMURA Iichiro
*大阪大学大学院医学系研究科病態制御医学病理学（修士）病理病態学
**大阪大学大学院医学系研究科内科系臨床医学内科学 内分泌，代謝内科学

はじめに

脂質の過剰摂取・運動不足という現代の生活習慣は，過剰な脂肪蓄積を惹起し，メタボリックシンドローム発症の基盤となる．メタボリックシンドロームとは，腹部肥満すなわち内臓脂肪蓄積を必須に，高血圧，脂質代謝異常，耐糖能異常を伴う動脈硬化易発症病態を包括的にとらえた疾患概念である．一方，全身の白色脂肪組織が極端に減少する全身性脂肪萎縮症（脂肪萎縮性糖尿病）も，よく似た代謝異常症候群，すなわちインスリン抵抗性，糖尿病，脂肪肝，高脂血症を呈する．これは全身の糖・脂質代謝の恒常性を保つうえで脂肪組織が重要な役割を担うことを示唆している．

脂肪組織は重量として身体の10%以上を占め，人体における主要なエネルギー備蓄臓器と考えられてきたが，近年の分子生物学的アプローチにより，アディポサイトカインと総称されるさまざまな生理活性物質を産生・分泌する生体内最大の内分泌臓器であることが知られ，肥満，とくに内臓脂肪蓄積により惹起されるアディポサイトカインの分泌異常が，肥満症，脂肪萎縮症，両疾病における病態やメタボリックシンドロームと密接にかかわることが明らかとなった．

本稿では，生活習慣病あるいはメタボリックシンドロームを考えるうえで重要な4つのアディポサイトカインについて述べる（図❶，❷）．

関連語
- メタボリックシンドローム/生活習慣病
- 脂肪組織/生理活性物質
- アディポネクチン/レプチン
- PAI-1/TNF-α

アディポサイトカイン

1）Plasminogen activator inhibitor-1 (PAI-1)

生体内における血液の凝固と線溶は種々の因子によりバランスが保たれるが，plasminogen activator inhibitor-1 (PAI-1)はプラスミノゲンアクチベータを抑制し，プラスミン生成を妨げ，フィブリンからのフィブリノーゲン分解産物生成を低下させる．つまり，PAI-1の増加は線溶活性を低下させ，血栓形成傾向に傾く．肥満者で静脈血栓症や心筋梗塞など，血栓性疾患の頻度が高いことは周知の事実であり，実際，脂肪蓄積，とくに内臓脂肪蓄積に伴い，脂肪組織PAI-1遺伝子発現量は上昇し，この上昇に連関して血中PAI-1濃度も上昇する[1]．血中PAI-1濃度は，肥満者，2型糖尿病患者で上昇し，血清トリグリセリド値とも相関する一方で，静脈血栓症や心筋梗塞患者でも上昇を認める．また，以前は血中PAI-1のおもな産生場所は肝臓であるとされていたが，脂肪蓄積に伴うPAI-1発現量は肝臓にて変化を認めず，内臓脂肪にて肝臓のレベルを凌駕する上昇を認めた[2)3)]．これにより，肥満形成に伴い，蓄積脂肪から直接分泌される血中PAI-1の上昇が，肥満と血栓性疾患とを直接結びつける因子

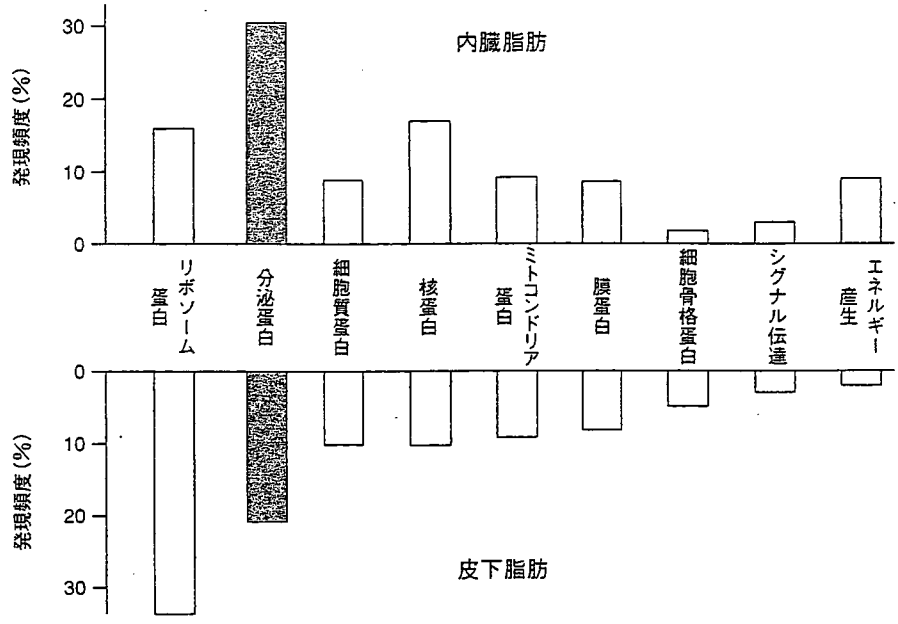

図❶ ヒト脂肪組織発現遺伝子解析(Body map project)

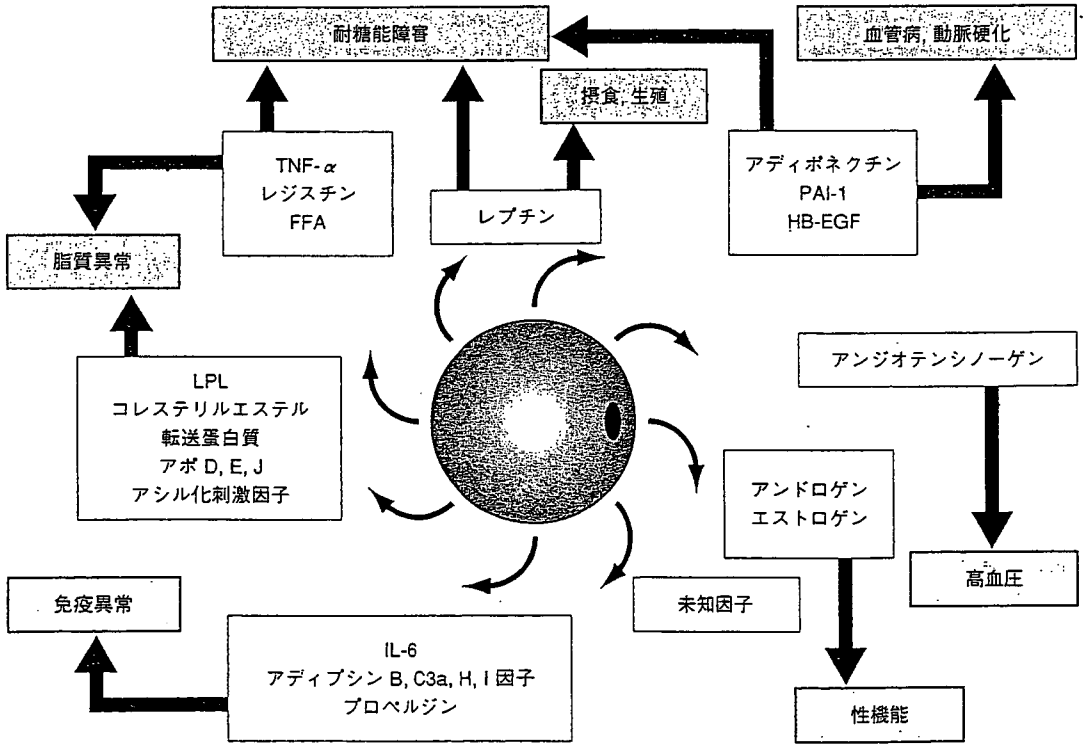

図❷ 脂肪組織由来生理活性物質(アディポサイトカイン)とその作用
FFA : free fatty acid, HB-EGF : heparin binding-EGF like growth factor, LPL : lipoprotein lipase, TNF-α : tumor necrosis factor-α , IL-6 : Interleukin-6, PAI-1 : plasminogen activator inhibitor-1.